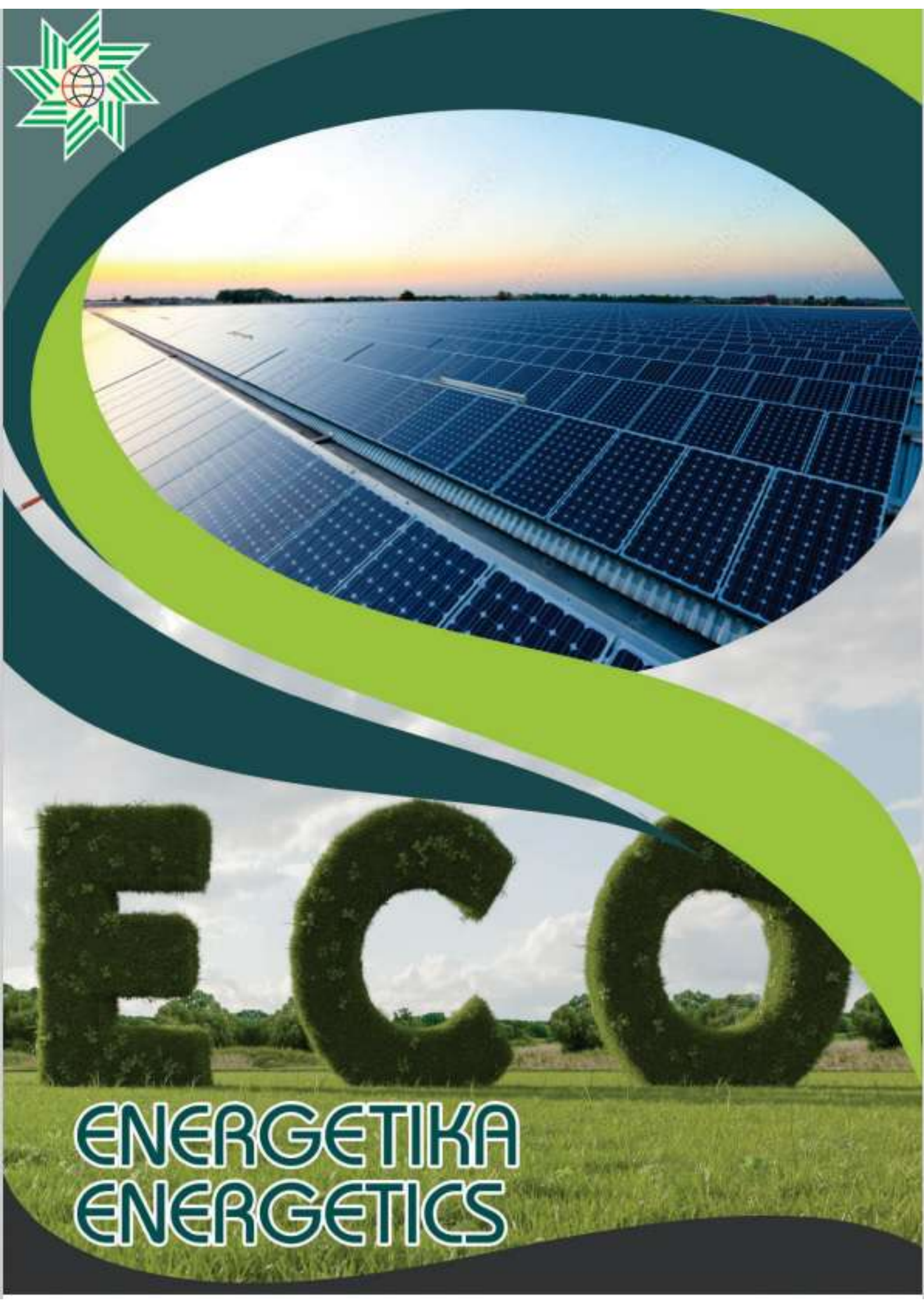
ECO
ENERGETIKA
ENERGETICS

Published from 2004
Ministry of Press and Information
of Azerbaijan Republic,
Registration number 3337, 07.03.2011

ISSN 1816-2126
Number 03, 2025
Section: English

ECOENERGETİCS

PUBLISHING OFFICE
5, M.Rahim, AZ-1073, Baku Azerbaijan

Tel.: 99412 538-23-70, 99412 538-40-25 Fax: 99412 538-51-22
E-mail: info@ieeacademy.org ekoenergetics@innovationresearch.az
Internet: http://ieeacademy.org www.innovationresearch.az

CONTENTS

A.A. Guliyev, A.V. Sharifova, I.I. Hasanov, **Ecoenergetics, vol. 30, № 3, pp.1-5, (2025)**
https://doi.org/10.69624/Ecoenergetics.2025.3.1

Application of methods for determining hardness at the yield limit and static processing of results

A.A. Guliyev, A.V. Sharifova, I.I. Hasanov

Azerbaijan State Oil and İndustry University, Baku, Azerbaijan,
aynur.sh84@mail.ru

Abstract. At present, the methods of investigating the mechanical properties of various materials are advantageous and important in all respects. Along with the positive progress of information on measuring hardness, which is one of the mechanical properties, by static and dynamic methods, there are still many problems that need to be solved. Obtaining such information is related to mechanical and non-mechanical methods of measuring hardness, and the mechanical method is reflected in static and dynamic methods. Among the issues being addressed are the development of a device for measuring the hardness of complex-shaped products in known hardness testers, the relationship between the stress state diagram in the zone of plastic deformation and uniaxial compression, the determination of the yield strength when characterizing the hardness of steel and hardening indicators. It has been studied that errors and deviations in determining the characteristics of properties are associated with loads, deformations and dimensions and increase the errors of the experimental results. Thus, when solving the problem of selecting the necessary small number of samples to estimate the average value of the mechanical property, errors in determining the average value and the average value with a given accuracy. In terms of the breadth of application, hardness testing, especially at room temperature, rivals the more common static tensile testing. This is explained by the simplicity, high productivity, absence of sample destruction, the possibility of assessing the properties of individual structural components and thin layers over a small area, and the easily established connection of the results of hardness determination with the data of other tests. It is shown that random errors are unavoidable but using probability theory methods they can be calculated and their influence on the true value of the measured quantity can be taken into account. An important characteristic of measurement accuracy is also the relative value of the mean square deviation - the variation coefficient.

Keywords: *Static methods, Deformation, Mechanical properties, Hardness, Yield strength, Static hardening, Coefficient of variation, Safety factor*

Corresponding author, email: aynur.sh84@mail.ru

1.Introduction

Hardness refers to the property of the surface layer of a material to resist elastic and plastic deformation or fracture under local contact action by another, harder and non-residually deformed body (indenter) of a certain shape and size. This formulation is not suitable for all existing hardness evaluation methods. The diversity of these methods and the different physical meaning of hardness numbers make it difficult to develop a common definition of hardness as a mechanical property. In different methods and under different test conditions, hardness numbers can characterize elastic properties, resistance to small or large plastic deformations, and material resistance to fracture [1,2]. Hardness testing, especially at room temperature, rivals the most common static tensile tests in terms of breadth of application. This is due to its simplicity, high throughput, lack of specimen fracture, ability to evaluate the properties of individual structural components and thin layers in a small area, and the easily established relationship of hardness results to other test data. When measuring hardness in the surface layer of the specimen under the indenter, a complex stress state close to volumetric compression occurs, which is characterized by the highest softness coefficient (a>2) compared to other types of mechanical tests. Therefore, it is possible to obtain “plastic” states, exclude fracture, and estimate the

hardness of virtually any metallic materials, including brittle ones [3].

Methods of hardness determination are divided into static and dynamic methods depending on the rate of load application, and by the method of load application - into indentation and scratching methods. The most common methods use static indentation of the indenter normal to the surface of the specimen [4].

The structure of real metals and alloys and the distribution of its defects are not the same even within a single sample. Therefore, the mechanical properties determined by structure and defects are, strictly speaking, different for different volumes of a single specimen. As a result, the characteristics of mechanical properties that we must evaluate in tests are average values that give a summary, mathematically the most probable characteristic of the entire volume of the specimen that takes part in the test. Even with absolutely accurate measurement of mechanical properties, they will not be the same from one sample of the same material to another. Instrumental errors in characterization of properties associated with the measurement of loads, strains, dimensions, etc., further increase the variation of experimental results. The main tasks of static processing of mechanical test results are estimation of the average value of properties and errors in determining this average, as well as selection of the minimum required number of specimens (or measurements) to estimate the average with a given accuracy [5,6].

The main tasks are the determination of yield hardness and static processing of mechanical test results and the reflection of the most complete information in the measurement processes.

2.Experimental detail

Application of the method of determination of yield strength $\sigma_{0,2}$ by hardness at the yield point $HB_{0,2}$ taking into account hardenability of the metal. This allows extending the limits of applicability of the method for various steels, including high-strength steels. The method is based on the relationship between the relative diameter of the yield stress indentation $(d/D)_{0.2}$ and the hardening index n included in the Meyer equation (Fig. 1). In establishing this relationship, the formula for determining the residual tensile elongation δ in the region of uniform deformation by the relative diameter of the indentation d/D* was used:

$$\delta = k\,(d/D)^m \qquad (1)$$

where d is the diameter of the indentation; D is the diameter of the spherical indenter; k, m are material constants.

The value $(d/D)_{0.2}$, corresponding to the elongation at yield strength δ=0.002, was determined from formula (11).

$$d/D_{0,2} = \sqrt[m]{0{,}002/k} \qquad (2)$$

Knowing the value $(d/D)_{0.2}$, it is possible to determine the corresponding load $P_{0.2}$ during indentation and calculate the yield hardness $HB_{0.2}$:

$$HB_{0,2} = \frac{2P_{0,2}}{\pi D^2[1-\sqrt{1-(d/D)_{0,2}^2}]} \qquad (3)$$

For a wide range of steels with widely varying levels of mechanical properties, a straightforward relationship was established between $\sigma_{0.2}$ and $HB_{0.2}$:

$$\sigma_{0,2}=0{,}33HB_{0,2} \qquad (4)$$

Thus, to estimate $\sigma_{0.2}$ by the proposed method, it is necessary to first determine the hardening index n based on the results of two indentations. Then, having found the value $(d/D)_{0.2}$ from the graph (Fig. 1), the ball should be indented until this indentation is obtained and the corresponding hardness $HB_{0.2}$ should be calculated, which is related to $\sigma_{0.2}$ by dependence (4).

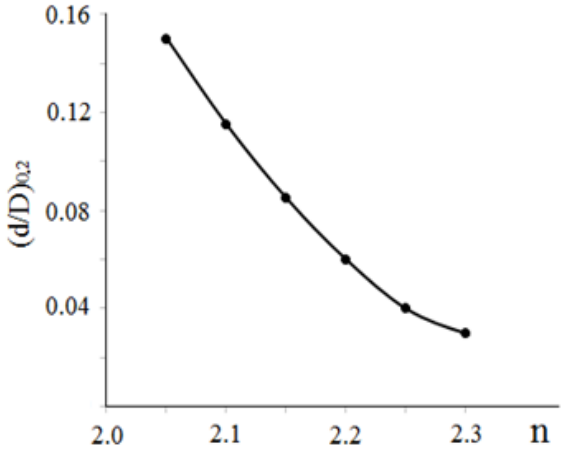

Fig. 1. Relationship between relative indentation diameter and hardening index

Experimental verification of the yield strength determination technique was performed on steels of different classes, heat-treated according to different regimes, as well as pre-stamped by cold plastic deformation by tension and compression. The maximum relative deviation of yield strengths determined by tensile and indentation did not exceed 7% [7].

Thus, the proposed technique can be recommended for determining the yield strength of steel by hardness.

When determining hardness by all methods (except microhardness), the total resistance of the metal to indenter penetration is measured, averaging the hardness of all available structural components. Therefore, the indentation obtained after the load is removed must be much larger in size than the grain sizes of the individual structural components (the diameter or diagonals of the indentation when measuring hardness vary from 0.1-0.2 to several millimeters). The inevitable differences in the structure of different parts of the sample lead to a scatter of hardness values, which is greater the smaller the size of the indentation [8].

These tasks are standard for statistical processing of any measurement results. The basic provisions of

methods for processing of measurement results and estimation of their errors are formulated in GOST 8.207-76 and are discussed in detail in various manuals. Here we will give only some elements of processing necessary for practically any mechanical tests. Specific features of processing the results of long-term high-temperature and fatigue tests are considered in the relevant works.

Usually, we determine the numerical value of a mechanical property from the results of several measurements. The set of n values of this property for the tested material is a statistical sample, which must be part of the general population of values of the property, the volume of which is theoretically infinitely large. The sample size in mechanical testing can vary widely: from 3-5 to several dozens and even hundreds of measurements when, for example, the results of tests of a product at a factory over a long period of time are processed [9].

The set of values x_i (i=1, 2, ..., n) of some property (e.g., hardness number or yield strength) determined because of tests usually obeys a normal distribution (Fig. 2). When the number of measurements n≤15, the normality of their distribution is not checked.

If n>15, GOST 8.207-76 requires such a check using special criteria.

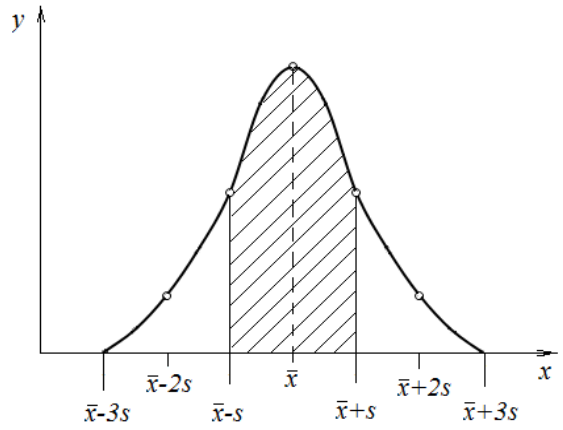

Fig. 2. Normal distribution curve

When the distribution of n individual values of a property is normal, its mean value x is calculated as the arithmetic mean in most cases

$$\bar{x} = \frac{1}{n}\sum_{i=1}^{n} x_i$$

Before determining the average value, it is advisable to check the set of obtained values for the presence of sharply standing out test results. These are usually the result of some gross error in measurement or the presence of major defects in the specimen. Such results should be excluded from further consideration.

In addition to gross errors, a distinction is made between systematic and random errors. Systematic errors are those whose nature is known and whose magnitude, at least in some cases, can be determined.

For example, if after the tests it turns out that the arrow of the force meter of the testing machine was displaced relative to zero, this will cause a systematic error in the determination of strength properties, which should be eliminated by introducing an appropriate correction.

Unfortunately, the magnitude of the systematic error cannot always be found, and sometimes we are not even aware of its existence, although its magnitude may be significant. For example, when testing a batch of porous samples, their properties may be underestimated by some approximately equal value in different samples, and, therefore, we will estimate the average value of the property with a certain systematic error. Systematic errors should be identified and accounted for wherever possible.

Errors of measurement results corrected by excluding gross errors and introducing corrections for systematic errors are called random errors. They are caused by the action of many factors, the influence of which on the measured property cannot be singled out and considered separately. Random errors are unrecoverable, but with the help of probability theory methods they can be calculated and their influence on the true value of the measured quantity can be considered [10]. To estimate the random error (error) of individual measurements, their deviation from the mean in the form of dispersion or mean square deviation (standard deviation) is determined:

$$s^2 = [1/(n-1)]\sum_{i=1}^{n}(x_i - \bar{x})^2$$

$$s = \sqrt{\frac{\sum_{i=1}^{n}(x_i - \bar{x})^2}{n-1}}$$

An important characteristic of measurement accuracy is also the relative value of the mean square deviation - the coefficient of variation $W = (s/\bar{x}) \times 100\%$.

All the listed characteristics of measurement errors do not yet say anything about the reliability of the obtained results. The most accurate estimate of the error value is given by the confidence interval or confidence limits in combination with the confidence probability.

Let us denote the true value of the measured property by x, the error of its measurement by Δx, and the arithmetic mean value that we obtain from the test results, $\bar{x}$.

Suppose now that the probability that $\bar{x}$ differs from x by an amount not greater than Δx is equal to: $P[-\Delta x<(x-\bar{x})<\Delta x]=a$.

The probability, a, is called the confidence probability, and the interval of values from $x-\Delta x$ to $x+\Delta x$ is called the confidence interval.

The confidence levels are usually taken as 0.9; 0.95 or 0.99. The size of the confidence interval is determined by the mean value $\bar{x}$, the standard deviation s and Student's t criterion, which depends on the chosen confidence level a and the number of measurements n: from $\bar{x} + (s/\sqrt{n})t$ to $\bar{x} - (s/\sqrt{n})t$.

From the analysis of the normal distribution function (see Fig. 2) it follows that about 66% of all measured values deviate from the mean value by less than s, 95% - by less than $2s$, and the probability of occurrence of deviation from the mean value of $\bar{x}$ by

3s is already negligible (0.003%). Therefore, the confidence limits of the measurement error of mechanical properties at a sufficient sample size do not exceed ±*3s* and are most often taken as ±*2s*.

In addition to the confidence interval of the random error of the measurement result, the confidence limits of the non-excluded systematic error must be calculated according to GOST 8,207-76. In the practice of mechanical testing this is rarely done, because it is considered that the unexcluded systematic errors are translated into random errors.

The average value of properties can be determined from a different number of measurements. Naturally, the average will be the closer to the true value of the defined value, the greater the number of measurements *n*. However, it is practically unprofitable to increase *n*, and people try to obtain the average with a certain accuracy at a minimum *n*.

One of the methods for determining a reliable mean at minimum *n* is based on an a priori specification of the possible spread of $\bar{x}$ within the confidence interval.

Let's assume for example that for a reliable average value of hardness number we consider it necessary to take such its value, which with confidence probability, *a*=0,99 will not deviate from $\bar{x}$ by more than 50 MPa (the last value is chosen based on the accuracy of the used method). Having determined *s* by several measurements *n* and gradually increasing their number, with the help of special tables we find such *n*, at which $ts/\sqrt{n} \leq 50MPa$.

If from preliminary experiments are known characteristics of the accuracy of this test method in relation to the tested material, the minimum required number of experiments can be determined a priori by the formula:

$$n = (mW_m^2K_w^2/J_P^2)\left(1 \pm 1/\sqrt{2m}\right)^2, \quad (5)$$

where m is the number of tests in the preliminary experiments; W_m is the difference between the maximum and minimum values of the results of preliminary tests; J_P is the maximum permissible deviation of the mean value from the true value set with probability P;

$$K_w = [t(m-1)]/d_m\sqrt{m},$$

where d_m - coefficient for estimating the mean square deviation by the number of measurements *m* (given in special tables).

Thus, the degree of reliability of determination of *n* by formula (5) depends mainly on the number *m* of preliminary tests.

When solving various problems, it is often necessary to compare some property of different materials. In this case, it is necessary to decide whether there is a significant difference between these properties, or their values are practically the same, considering the error of determination and the number of measurements. Sometimes the number of measurements is not considered, which leads to an incorrect conclusion. For example, the difference between x_1=10 and $\bar{x}$=12 is considered insignificant because s_x>2. In fact, the difference between the averages can be significant if *n* was large enough.

The comparison of two mean values can be performed using different static criteria. Suppose we have two averages

$\bar{x}_1$ and $\bar{x}_2$ determined from n_1 and n_2 measurements with mean square deviations s_1 and s_2, respectively. If we combine all measurements into one sample, the mean square deviation of a single value will be:

$$s_m = \sqrt{\frac{(n_2-1)s_1^2+(n_2-1)s_2^2}{(n_1-1)+(n_2-1)}}.$$

If using Student's *t* - criterion:

$$(\bar{x_1} - \bar{x_2}) \leq ts_m\sqrt{\frac{n_1+n_2}{n_1n_2}}, \quad (6)$$

then both series of measurements belong to the same general population and, therefore, the difference between the mean values of the properties is insignificant. If the left part in equation (6) is greater than the right part, then the differences between the averages are not random (of course, with some confidence probability, *a*, which determines the value of *t* - criterion). Mechanical properties are often used in industry to assess the quality of metal materials and metal products. Standards and technical specifications for many metal products stipulate the minimum permissible (guaranteed) values of certain individual mechanical properties or a combination of them. Therefore, when checking the quality of such products at the factory, it is necessary to determine the relevant properties and make sure that their minimum values are not lower than the required level.

In accordance with the standard [11] it is necessary that the smallest value $x_{(1)}$ of the measured property of the samples from the controlled batch (sample) was not less (sometimes the product suitability is assessed "from above" - under the condition $x_{(n)}<C$, where $x_{(n)}$ is the largest value of the property (e.g. hardness) in the sample) some acceptance value *C*: $x_{(1)}\geq C$.

Acceptance value is calculated as $C=C_0+\gamma s$, where C_0 - norm (minimum required value of the property), given in the normative and technical documentation for the product; γ - scattering reserve coefficient for mean square deviation, which is determined by a special Table 1. The meaning of the coefficient is that it, depending on the sample volume and responsibility of the controlled product designation, determines a different value of the "reserve" of ensuring the minimum permissible value of the property (C_0).

For the most critical products it is recommended to use γ values given in Table 1 lines with indices 1.1, 1.2, for other types of products - in lines 2.1, 2.2. When controlling large batches (more than 100 products) use the values of γ in the rows of Table 1 with indices 1.2 and 2.2. it is necessary to strive to reduce the scattering margin γs.

Table 1. Values of the dissipation factor

Control level index	Value of γ for sample size *n*									
	1	2	3	4	5	6	7	8	9	10
1.1	2.9	2.4	2.0	1.7	1.5	1.4	1.2	1.1	1.1	1.0
1.2	2.9	2.0	1.6	1.3	1.2	1.0	0.9	0.8	0.7	0.6
2.1	1.6	2.1	1.7	1.5	1.3	1.2	1.1	1.0	0.9	0.8
2.2		1.8	1.4	1.1	0.9	0.8	0.7	0.5	0.5	0.5

For this purpose, work should be carried out to increase the homogeneity of the values of mechanical properties of products, i.e. to reduce the mean square deviation s. For a given value of s, the reduction of the scattering margin can be achieved by increasing the volume of the control sample (see Table 1).

3.Conclusion

Analyzing the classification of hardness determination methods divides it into parts such as static and dynamic methods. The most common method, in which static indentation of the indenter of the sample surface is used. Experimental verification of the method of yield strength determination was performed on steels of different classes. The static evaluation of hardness on yield strength of different materials and products has maximum regularity. It is determined that the results of the characteristic of mechanical properties, which are evaluated in tests, are average statistical values, giving a summary, mathematically the most probable characteristic of the entire volume of the specimen. It is shown that random errors are unrecoverable, but with the help of probability theory methods they can be calculated and their influence on the true value of the measured value can be considered. An important characteristic of the accuracy of measurements is also the relative value of the mean square deviation - the coefficient of variation. Regularities of normal distribution of the dependence of a set of values determined in the test results of static processing of mechanical tests (hardness and yield strength) reflects the most complete information in the processes of hardness measurement.

References

[1] Q. V. Klevchov, L.R. Botvina, N.A. Klevchova, L.V. Limar, Fraktodiaqnostika razrusheniya metallicheskix materialov i konstrukchiy. M.: MİSis, 2007, 264 p.;

[2] A. A. Bolshakov, R. N. Karimov, Metodi obrabotki мnoqomernix dannix i vremennix ryadov: [uchebnoe posobie po magisterskoy proqramme 550209 "Avtomatizachiya nauchnix issledovaniy, ispitaniy i eksperimenta" napravleniya 550200- "Avtomatizachiya i upravlenie", po napravleniyam 230100 (654600) - "Informatika i vichislitelnaya texnika"] M. Qoryachaya liniya - Telekom 2007, 522 p.;

[3] E.S. Lopatina, Mexanicheskie svoystva metallicheskix materialov. Laboratorniy praktikum: uchebnoe posobie dlya studentov vuzov, obuchayushixsya po napravleniyu 150400.62 "Metallurgiya" / E. S. Lopatina, A. A. Kovaleva, V. I. Anikina; Sib. fedr. un-t, In-t chvet. Metallov i materialovedeniya - Krasnoyarsk: SFU, 2015, 95 p.;

[4] A. V. Ploxov, Fizicheskie i mexanicheskie svoystva: uchebnik / A. V. Ploxov, A. I. Popelyux, N. V. Plotnikova — Novosibirsk: NQTU, 2018. 342 s.;

[5] A. A. Lebedev, N. R. Muzyka, V. P. Shvets, On options of improving reliability of material hardness assessment methods, Strength Mater., 43, No. 3, 2011, pp. 237–246. https://doi.org/10.1007/s11223-011-9291-z

[6] N. R. Muzyka, Influence of the anisotropy of sheet materials on the accuracy of measuring of the Vickers hardness, Strength Mater., 39, No. 2, 2007, pp. 211–218. https://doi.org/10.1007/s11223-007-0027-z

[7] V. V. Kharchenko, N. P. Rudnitsky, O. A. Katok, et al., Installation for determining the mechanical characteristics of structural materials by instrumented indentation, in Reliability and Durability of Machines and Structures [in Russian], Issue 28, Kyiv (2007), pp. 140–147.

[8] M. R. Muzyka, Experimental Determination of the Optimal Hardness Testing Method Depending on the Material's Physical and Mechanical Properties. Strength Mater., 55, 2023, pp.1181–1191. https://doi.org/10.1007/s11223-024-00608-w

[9] P. Men, Sh. Dong, X. Kang, Sh. Yan, Zh. Cheng, R. Lv. Research on the method of quantitative evaluating material hardness and tensile strength by critically refracted longitudinal wave. Applied Acoustics, Volume 159, February 2020, 107-105. https://doi.org/10.1016/j.apacoust.2019.107105

[10] O. A. Katok, M. R. Muzyka, V.P. Shvets', et al., "Determination of hardness of high-strength steels by the Brinell method. Part 1. Improvement of measurement accuracy," Strength Mater, 53, No. 6, 902–908 (2021). https://doi.org/10.1007/s11223-022-00358-7

[11] GOST-22013-76 "Staticheskiy priemochniy kontrol metallicheskix materialov i izdeliy po naimenshemu znacheniyu mexanicheskoy xarakteristiki"

S.A. Hasanova, E.N. Hajiyev, Ecoenergetics, vol. 30, № 3, pp.6-9, (2025)
https://doi.org/10.69624/Ecoenergetics.2025.3.6

Impact of Process Safety Management on Oil Production Efficiency in Azerbaijan

S.A. Hasanova, E.N. Hajiyev

Azerbaijan University of Architecture and Construction

Seynure.ibrahimova@gmail.com

Abstract. The oil and gas industry in Azerbaijan is crucial to the economy but faces high operational risks. Effective Process Safety Management (PSM) is key to maintaining production efficiency. The paper examines how PSM elements like mechanical integrity, safety culture, change management, emergency preparedness, and digital monitoring impact operational reliability in both offshore and onshore facilities. The research shows that strong PSM implementation correlates with increased uptime, equipment availability, and fewer unplanned shutdowns. Facilities following organized PSM frameworks demonstrate better discipline, risk identification, and quicker recovery from abnormal events. Predictive maintenance and data-driven monitoring in the Caspian region have reduced downtime and extended asset life. In Azerbaijan, where international operators and SOCAR manage large-scale facilities, PSM is integrated into daily operations, driving business efficiency rather than just regulatory compliance. The paper concludes that improving PSM maturity is essential for both safety and long-term economic competitiveness.

Keywords: Process Safety Management (PSM), Risk Identification, Digitalization, Energy Security.

Corresponding author, email: Seynure.ibrahimova@gmail.com

1.Introduction

Oil production is a cornerstone of Azerbaijan's national economy, significantly contributing to export revenues and driving industrialization. As extraction technologies evolve and become more complex, the potential for operational risks has also increased. These risks may arise from a variety of sources, including equipment malfunctions, process deviations, and loss of containment. Such disruptions not only jeopardize the safety of workers but also compromise the efficiency of production processes and the overall profitability of the sector. Given the heightened operational risks, Process Safety Management (PSM) has emerged as a critical framework for improving the reliability, consistency, and safety of production operations in Azerbaijan's oil industry. PSM involves the application of systematic processes, tools, and technologies aimed at ensuring that oil production activities are carried out safely, efficiently, and with minimal risks to personnel and the environment. Globally, industries that have implemented organized and comprehensive PSM systems have reported substantial improvements in production uptime, reduced occurrences of accidents, and a decrease in unplanned shutdowns. A well-executed PSM system identifies potential hazards, enforces rigorous safety protocols, and ensures that equipment is maintained in optimal condition, which collectively help to reduce the likelihood of accidents and system failures. Additionally, organizations that follow structured PSM frameworks are better equipped to respond to abnormal situations, ensuring faster recovery and minimizing production downtime. When operational risks are mitigated, the potential losses associated with accidents or unplanned shutdowns are also minimized. This proactive approach to managing risks not only enhances operational reliability but also safeguards the financial health of the company, ensuring the long-term sustainability of oil production in Azerbaijan. In summary, the implementation of effective PSM systems in the oil production sector plays a pivotal role in minimizing risks, maximizing uptime, and improving the overall safety and efficiency of operations. This approach is crucial for maintaining Azerbaijan’s position as a major player in the global oil industry, while also ensuring the continued contribution of the sector to the nation’s economic growth [1-4].

2.Experimental detail

2. Background of Process Safety Management

Process Safety Management (PSM) is a structured management method, which has been designed to detect and control hazards arising due to the high-risk

industrial practices, especially the ones, which involve the use of hazardous chemicals [5]. Present PSM model is based on OSHA 1910.119, which codified process safety requirements after significant industrial accidents that have taken place in the late twentieth century [6]. Currently, both the Center for Chemical Process Safety (CCPS) and the American Petroleum Institute (API) have PSM frameworks that are widely utilized across the oil and gas industry across the world [7].

Diagram 1. The 14 Fundamental Elements of Process Safety Management.

Empirical studies in process safety have suggested that significant industrial accidents are usually associated with latent organizational failures or a lack of mechanical integrity or procedural shortcomings, as opposed to the independent actions of operators [8].

3. Theoretical Link Between PSM and Production Efficiency

The efficacy of production in the context of oil and gas activities depends on the reduction of the disruption and high equipment availability [9]. The use of Process Safety Management (PSM) helps achieve this goal through the mitigation of unplanned outage through the organization of maintenance, stringent risk evaluation, and process discipline implementation [10]. Improved identification of hazards and the sophisticated decision-making processes will help organizations to respond before the situation deteriorates, thus preventing failures capable of crippling the production outputs [11]. An effective PSM system is one that is executed effectively at the same time, it helps to reduce the chances of huge accidents, hence preventing lengthy production halt, unilateral shutdowns, and costly remediation efforts [12].

4. Impact of PSM on Production Efficiency

4.1 Improving Safety Culture and Operational Discipline.

The empirical research points out that the strong safety culture improves the operational reliability through the decrement of the procedural violations and the near miss cases [13]. In Azerbaijan, behavioral safety programs, such as the BP programmer, Safety Leadership, and the SOCAR programmer, 0 Harm, have been shown to have quantifiable reductions in process deviations in Azerbaijan [14].

Image 1. The Impact of Downtime on Key Performance Dimensions Relevant to PSM and Production Efficiency

4.2 Minimization of Equipment Failure and Mechanical Integrity.

One of the principles of Process Safety Management (PSM) is the mechanical integrity that increases the resilience of the most crucial equipment by conducting a regular inspection, testing, and preventive maintenance of the equipment [15]. Caspian Sea offshore installations are faced with increased corrosion and environmental stressors and thus, integrity management becomes essential in ensuring production stability [16].

4.3 Operational Reliability and Management of Change (MOC).

Ineffective Management of Change (MOC) activities have been identified as one of the leading cause of process uproar and equipment breakdowns on an international level [17]. Azerbaijani companies that have improved their MOC approval recommendations have documented smoother transition of operations and less post-change upheavals [18].

4.4 Preparedness to Emergencies and Reduction of Incidents Impact.

An advanced PSM model will include all-inclusive emergency response planning, which will significantly reduce downtime after the occurrence of abnormal events [19]. Quickly containing a swift incident prevents it from blowing out of proportion and reduces the recovery time operational period [20].

4.5 Automated Data-Based Surveillance and Predictive Maintenance.

Digitalized PSM architectures that apply predictive

analytics and sensor-based monitoring systems allow detection of anomalies before equipment failure in advance before failure happens [21]. Azerbaijan offshore locations that have adopted predictive maintenance have registered maintenance-related shutdowns reductions of 1520 [22].

5. Case of Azerbaijan's Oil Production Sector

5.1 Structural Challenges

The oil industry in Azerbaijan is marked by old infrastructure and operation of new deep-water platforms which are operated by international consortia^[23]. These circumstances foster diverse levels of safety maturity among assets, which, in turn, affect the uniformity of process safety management (PSM) [24].

5.2. SOCAR and International Practices of Operators.

The international operators like BP, TotalEnergies, and Equinor use PSM systems which are following the provisions of API RP 750, OSHA 1910.119 and CCPS guidelines, as of [25]. In recent times, SOCAR has stepped up pace in reforming the safety governance by improving integrity management, implementing digital monitoring systems and supplying workforce training [26].

5.3 Empirical Observations

Evidence on the impact of sound PSM practices on facilities is provided by the data on the results of the implementation of these practices by AREA, SOCAR, and other international operators which show that facilities with an effectively implemented PSM practices are characterized by: a 2030% reduction in the number of unplanned shutdowns, a 15% improvement in equipment availability, a 25% decrease in the amount of the maintenance backlog, and as many as 40% fewer disruptions associated with an incident [27].

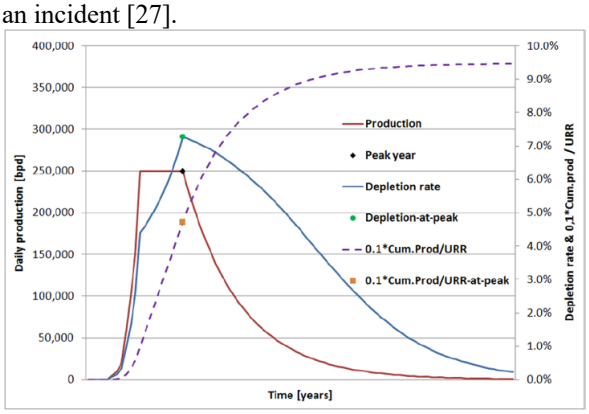

Figure 1. Illustration of Decline Patterns in Oil Fields Relevant to Operational Efficiency and Safety Management.

The findings of the present investigation are empirical, thus creating a clear and consistent relationship between the maturity of Process Safety Management

The current study confirms that Process Safety (PSM) systems and the efficiency of production in the oil industry of Azerbaijan. The findings also indicate that PSM should be redefined as something more than a compliance-based safety system, and it should come up as an essential pillar of operations optimization. Websites with a high level of PSM maturity are characterized by increased organizational resilience, more balanced operational processes, and statistically significant decrease in risk related downtime. These results are in line with the study on risk management and mechanical integrity in other countries that suggests a significantly higher long-term asset performance of firms that invest in organized risk management and mechanical integrity [28]. One of the most striking arguments that are brought into the light of the analysis is the interdependence of technical and cultural aspects of PSM. Although mechanical integrity, digital monitoring and predictive maintenance are proven to decrease the failures rate, the development of the strong safety culture is equally important in maintaining the production chain. The behavioral safety programmer put in place by the international operators and SOCAR demonstrate that once the employees internalize the values that relate to safety then reporting is more transparent, there is an increase in procedural compliance, and the disruptions caused by human errors are reduced. This cultural aspect therefore increases the effectiveness of technical controls, which creates a more integrated and consistent operational setting [29]. In addition, the paper highlights that Management of Change (MOC) is one of the most powerful but frail elements of PSM in Azerbaijan. Various operational accidents around the world and several of them recorded in the Caspian region are rooted in unverified changes in technical or operating procedures. Improving MOC processes will thus most likely contribute to a considerable efficiency increase through the reduction of post-change process deviation. Although this gradual adherence to digital operations and automated systems of approval is a positive move, it is crucial to insist on the adoption of these measures in all facilities. The paper also brings to light the growing significance of digitalization in PSM structures. With the continuation of the aging of the oil infrastructure in Azerbaijan, especially with the old offshore platforms that are highly maintained and require fundamental maintenance, digital tools, including real-time asset integrity monitoring, root-cause analytics, and predictive algorithms, are new channels of active risk reduction. Improvement of the safety results is not the only way in which the combination of these technologies supports production planning, maintenance prioritization, and operational forecasting [30]. Taken together, the evidence points to the fact that PSM is a safety-netting element and a performance amplifier. The twofold benefits of preventing accidents and increasing efficiency make PSM essential to long-term industrial and economic purposes of Azerbaijan [31].

5.Conclusion

Management (PSM) is the essential component of the

process of optimization of production efficiency of the oil industry in Azerbaijan. Using the experience of other countries, empirical evidence, and evidence based on cases, an effective PSM implementation will prove to lessen operational risk, reduce the number of unexpected shutdowns, and increase equipment availability. Such returns are not only due to technical controls that include mechanical integrity, predictive maintenance but also organizational determinants, i.e. safety culture, competence development, and effective communication [32]. In national setting where production of hydrocarbons remains one of the staples of the economic stability and export income, the strategic importance of PSM becomes even more pronounced. The strong safety governance is the key not only to the safety of workers and the elusive of disastrous accidents, but also to the continuity of production and the guarantee of the long-term economic support. The analysis shows that companies in Azerbaijan that invest in more developed monitoring systems, organized training systems and proactive maintenance plans achieve better performance results compared to companies using less developed systems. In the long term, the maturation of PSM needs to be strategically focused at all the levels of the Azerbaijan oil production infrastructure. To achieve this goal, it is necessary to invest in digitalization and integrate the best practices of the world, strengthen regulatory control, and enhance the competencies of operators, as well as their continuous growth. Moreover, the harmonization of safety values among the international companies and the local ones would lead to the creation of a single risk management approach within the industry. Finally, PSM should be considered as an effective economic tool. This guarantees national energy security and long-term industrial competitiveness by reducing the uncertainty, stabilizing operations and extending the lifespan of assets, to ensure safer working conditions. In the case of Azerbaijan, this development of PSM capabilities will be the key to maintaining the efficiency of production in a more complex and technologically challenging global energy environment.

References

[1] BP, *Safety and Operational Excellence Report, 2023*.
[2] S. Mannan, *Lees' Loss Prevention in the Process Industries*. Elsevier, 2012.
[3] CCPS, *Guidelines for Risk Based Process Safety*. Wiley, 2020.
[4] API, *Recommended Practice 750: Management of Process Hazards*. American Petroleum Institute, 2019.
[5] OSHA, *Process Safety Management of Highly Hazardous Chemicals – 29 CFR 1910.119, 2019*.
[6] T. Kletz, *Learning from Accidents*. Gulf Professional Publishing, 2001.
[7] T. Aven, *Risk Analysis*. Wiley, 2015.
[8] A. Hopkins, *Failure to Learn: The BP Texas City Disaster*. CCH Australia, 2009.
[9] BP Caspian, *Production Efficiency Overview*. BP Azerbaijan, 2022.
[10] J.E. Skogdalen,, J.E. Vinnem, Quantitative Risk Analysis Applied to Offshore Installations, *Safety Science*, 50, 2012.
[11] J. Erikson, Human Factors in Process Safety, *Journal of Loss Prevention*, 54, 2018.
[12] CCPS, *Mechanical Integrity for Fixed Equipment in the Process Industries*, 2018.
[13] J. Reason, *Managing the Risks of Organizational Accidents*. Ashgate, 1997
[14] SOCAR, *Health, Safety & Environment Annual Report*, 2003.
[15] API, *Safety Culture Assessment Guide*, 2017
[16] ABS (American Bureau of Shipping), *Corrosion and Offshore Infrastructure Integrity*, 2020.
[17] CCPS *Management of Change: Best Practices*, 2017.
[18] S.A. Hasanova, Compared the efficiency of TiO_2 and N-doped TiO_2 to degrade BTEX. Advanced Physical Research, 3(3), 123-128, 2021.
[19] S. A. Hasanova, F. G. Aliyev, M. A. Gurbanov, Y. D. Jafarov, Study of the chemical processes occurring in the gas phase because of photolysis of produced waters under the ultraviolet rays influence. PPOR, 24(4), 623-630, 2023. DOI:
[20] S. Hasanova Analysıs of gases produced from photolysıs of heterogeneous phase formed waters under the ınfluence of ultravıolet radıatıon. Scientific Works Journal. №2, 2024.
[21] Equinor *Operational Safety & Change Management Performance Report*, 2021.
[22] NFPA *Fire Protection Handbook, 2019*.
[23] ICS/OCIMF, *Effective Emergency Response in Oil & Gas Installations, 2018*.
[24] Siemens Energy, *Predictive Maintenance Technologies in Oil and Gas* 2021.
[25] DNV GL, *Digitalization and Predictive Integrity Management in Offshore Operations*, 2020
[26] EBRD, *Azerbaijan Oil Sector Infrastructure Assessment*, 2022.
[27] Wood Mackenzie, *Caspian Basin Asset Performance Overview*, 2021.
[28] TotalEnergies, *Safety and Process Integrity Report*, 2022.
[29] SOCAR, *Strategic Modernization and Safety Reform Programme*, 2021.
[30] AREA Azerbaijan, *Operational Safety Performance Review*, 2023.
[31] OECD, *Safety Culture and Efficiency in High-Risk Industries*, 2019.
[32] IOGP, *Process Safety Fundamentals for Upstream Operations,* 2020.
[33] World Bank, *Azerbaijan Energy Sector Policy Review*, 2020.
[34] BP, *Process Safety Report: Caspian Assets, 2021*.
[35] UNECE, *Industrial Safety and Risk Management in Eastern Europe & Caspian Region, 2022*.

M. I. Maharramov, Ekoenergetics, vol. 30, № 3, pp.10-14, (2025)
https://doi.org/10.69624/Ecoenergetics.2025.3.10

A Meteonorm-Derived Monthly Solar Resource and Climate Baseline for Photovoltaic Planning in Aghdam city

M. I. Maharramov

Azerbaijan University of Architecture and Construction

maharramovmobil@gmail.com

Abstract. This study presents a comprehensive monthly summary of solar energy resources and climate conditions for Aghdam, Azerbaijan, using data compiled from Meteonorm. Six key variables relevant to photovoltaic planning are included: global and diffuse horizontal irradiation, mean air temperature, precipitation, sunshine duration with astronomical daylength, intra-monthly ranges of daily irradiation, and monthly series of daily maximum and minimum temperatures. The annual total for global irradiation is 1530 kWh per square meter, and diffuse irradiation is 745 kWh per square meter, with the highest values occurring in June and July, and the lowest in December and January. The variability of daily irradiation within months is significant, especially during summer and winter. Monthly mean air temperatures range from 3.6 °C in January to 27.0 °C in July, while the average difference between daytime and nighttime temperatures is 8.8 °C. Annual precipitation totals 1271 millimeters, with December being the wettest month and January the driest. Together, these metrics define the seasonal patterns and variability of Aghdam's solar resource and climate, providing a reliable baseline for photovoltaic system design, technology selection, performance modeling, and maintenance planning.

Keywords: Tilted-plane irradiation; Photovoltaic yield; Clearsky model; PV system sizing; GHI variability.

Corresponding author, email: maharramovmobil@gmail.com

1.Introduction

Since 2000, the cost of producing electricity from photovoltaic (PV) modules has decreased substantially, making PV power increasingly competitive with electricity generated from fossil fuels. At the same time, various organizations around the world have introduced financial incentives to encourage the adoption of low-carbon energy sources. As a result, the total installed PV capacity worldwide increased from 40.2 GW in 2010 to 580.2 GW in 2019, representing a 14.4-fold growth. During this period, the combined capacity of all renewable energy sources also doubled, rising from 1,226.6 GW to 2,536 GW [6]. Solar radiation measurements are widely used to assess solar system performance and financial viability, guide the architectural design of passive heating, cooling, and daylighting features, and quantify resources for agricultural and forestry planning [1]. In 2022 Europe added 46.1 GW of new solar photovoltaic (PV) capacity, and annual additions are forecast to climb to about 120 GW by 2027 (SolarPowerEurope, 2023). Globally, the IEA (2021) projects that solar PV will contribute roughly half of all renewable power expansion between 2021 and 2026 [5]. Reliable solar energy planning depends on accurate, location-specific characterization of the resource and the local climate. Bankable assessments for photovoltaic deployment typically require not only estimates of monthly global horizontal irradiation, but also information about the share of diffuse radiation, the thermal regime that influences module efficiency, precipitation patterns relevant to soiling and operations, and the timing of daylight and bright sunshine that governs production windows. For cities undergoing rapid development, these inputs guide technology choice, array sizing, expected yield, and grid integration studies. Aghdam City, Azerbaijan, lacks a consolidated, publicly documented profile of these parameters at the monthly scale. While national or regional summaries are often used as proxies, such generalizations can introduce bias when translated to a specific urban site. A reproducible approach rooted in a standardized climatological database is therefore needed to provide a consistent basis for engineering calculations and comparative analyses. Metronome offers a practical solution for this purpose because it synthesizes long-term ground observations and satellite products into internally consistent time series and climatologist. Using a single, well-defined source

helps avoid artefacts that may arise when mixing stations, periods, or methodologies, and allows the derivation of secondary metrics that are widely used in solar engineering without additional homogenization steps. In this study, a compact but comprehensive set of variables from Meteonorm for Aghdam is assembled to describe the city's solar resource and its co-varying meteorology at the calendar-month scale. The focus is on six elements that are directly relevant for photovoltaic planning: monthly totals of global and diffuse horizontal irradiation, monthly mean air temperature, monthly precipitation, monthly mean daily sunshine duration alongside astronomical daylength, intra-monthly ranges of daily global irradiation, and monthly series of daily maximum and minimum air temperatures. Together, these variables characterize the magnitude and seasonality of incoming energy, the expected variability of day-to-day production within a month, and the thermal and hydrological context that conditions system performance and maintenance. The analytical choices are guided by common design questions. The diffuse fraction informs expectations about the relative benefits of tracking versus fixed-tilt configurations and helps anticipate performance under frequent cloudiness. Monthly and seasonal temperature statistics provide first-order estimates of temperature-induced efficiency losses and of potential heat-related curtailments. Precipitation totals, while not a proxy for aerosol loading, are a practical indicator for cleaning requirements, access, and operational risk. Sunshine duration and daylength translate directly into potential operating hours, and daily irradiation ranges within each month help quantify the variability that underpins inverter loading, storage sizing, and grid interaction. As the largest nation-state in the South Caucasus, the Republic of Azerbaijan has substantial potential to develop and deploy renewable energy sources to address climate change–related environmental challenges and improve national environmental conditions [2]. The objective of the paper is therefore descriptive and diagnostic rather than predictive. The six variables for Aghdam are compiled and presented, a small set of secondary metrics standard in solar resource assessment are derived, and their monthly and seasonal behavior is summarized. The resulting dataset and statistics provide a transparent baseline for subsequent performance modelling, technology comparison, and planning decisions in the city context.

2.Experimental detail

Many solar radiation models have been developed to estimate irradiance when direct measurements are unavailable or unsuitable. A widely accepted classification system for these models only emerged after Gueymard and Myers (2008) introduced nine criteria for categorization. According to their framework, a transposition model (criterion 8) uses measured or modeled irradiance components on the horizontal surface as inputs to calculate radiation on surfaces of different orientations. Meteonorm 8 employs this type of transposition approach, generating reliable irradiance data for various locations even in the absence of site-specific measurements [4]. Meteorological and solar resource data for Aghdam City, Azerbaijan, were obtained from the Meteonorm database (version and provider details in full reference), which synthesizes long-term climate normals from ground stations and satellite observations [3]. The analysis encompasses six key variables relevant to solar energy assessment: monthly global and diffuse horizontal irradiation, monthly mean air temperature, monthly precipitation, monthly sunshine duration and astronomical daylength, intra-monthly ranges of daily global irradiation, and monthly series of daily maximum and minimum air temperatures. All data are provided as monthly aggregates, except where daily ranges are explicitly reported, and follow the standard units and conventions of Meteonorm: irradiation in $kWh \cdot m^{-2}$ (per month or per day), air temperature in degrees Celsius (°C), precipitation in millimeters (mm), and time-related parameters in hours. Irradiation values refer to a horizontal surface, with diffuse irradiation representing the sky component exclusive of direct solar beam, and daylength based on astronomical sunrise and sunset. All variables are reported for the standard reference period and location as defined in Meteonorm, ensuring consistency and reproducibility in subsequent analyses. Meteonorm monthly totals of global horizontal irradiation (Gh) and diffuse horizontal irradiation (Dh) were exported for Aghdam in $kWh \cdot m^{-2} \cdot month^{-1}$ and used without further transformation. We report only Gh and Dh on the horizontal plane (no decomposition into additional components), and for each month compute the diffuse fraction to characterize the sky-share of the total. The exact monthly inputs used in subsequent analyses are:

Month	Diffuse radiation (kWh/m²)	Total (kWh/m²)
January	30	70
February	40	80
March	60	120
Aprel	80	145
May	90	180
June	100	200
July	90	190
August	85	180
September	60	135
October	45	95
November	35	70
December	30	65

From these, we derive the annual sums $\sum Gh = 1530$ and $\sum Dh = 745$ $kWh \cdot m^{-2} \cdot year^{-1}$ and the annual diffuse fraction $f_{d,\Sigma}=48.7\%$. For seasonal context (DJF, MAM, JJA, SON), the totals are Gh = 215, 445, 570, 300 and Dh = 100, 230, 275, 140 $kWh \cdot m^{-2}$, respectively; monthly f_d ranges from ≈42.9% (January) to ≈55.2% (April), providing the basis for comparative

interpretations in the Results. Monthly mean air temperature data for Aghdam were obtained from Meteonorm, which estimates 2 m screen-height temperatures using interpolated long-term ground station records and satellite-based inputs. For each calendar month, Meteonorm provides the average of daily mean temperatures, resulting in a continuous annual temperature profile representative of local climatic conditions over the baseline period. The extracted dataset includes twelve monthly means, ranging from 3.6 °C in January to 27.0 °C in July. The specific values for each month are as follows: 3.6, 4.7, 9.0, 13.4, 19.4, 24.5, 27.0, 26.6, 21.7, 15.5, 9.2, and 4.9 °C, listed from January through December. Seasonal averages were calculated by grouping calendar months into the standard meteorological seasons: winter (December to February, DJF), spring (March to May, MAM), summer (June to August, JJA), and autumn (September to November, SON). The resulting seasonal mean temperatures are 4.4 °C for DJF, 13.9 °C for MAM, 26.0 °C for JJA, and 15.5 °C for SON. The annual mean temperature, calculated as the arithmetic mean of all 12 monthly values, is 15.0 °C. The intra-annual temperature amplitude, defined as the difference between the warmest month (July, 27.0 °C) and the coldest month (January, 3.6 °C), is 23.4 °C, reflecting significant seasonal variability. All temperature values are presented to one decimal place, matching the precision of Meteonorm's outputs. These data establish the thermal context for subsequent analyses of photovoltaic performance, including temperature-dependent efficiency losses and seasonal energy yield, and serve as a reference for comparative climatology.

Month	Min [°C]	Max [°C]
January	0	16
February	-3	17
March	0	22
Aprel	2	26
May	10	30
June	15	35
July	18	38
August	20	37
September	17	33
October	7	26
November	2	21
December	-1	17

Monthly precipitation totals for Aghdam were extracted from Meteonorm as calendar-month aggregates expressed in millimeters per month (mm·month^{-1}). Precipitation represents the equivalent liquid depth of all forms of precipitation as provided by Meteonorm. No gap filling or bias correction was applied. All computations retained the dataset's native monthly resolution and precision. The monthly series (January to December) used in subsequent analyses is: 60, 80, 118, 120, 145, 140, 80, 70, 105, 110, 75, 168 mm·month^{-1}. From these values we calculated the annual total as 1271 mm·year^{-1} and the mean monthly precipitation as 105.9 mm. The wettest month is December (168 mm) and the driest month is January (60 mm), identified by the monthly maximum and minimum, respectively. Seasonal totals were obtained by summing calendar months into standard meteorological seasons: winter (DJF), spring (MAM), summer (JJA), and autumn (SON). The resulting totals are DJF 308 mm, MAM 383 mm, JJA 290 mm, and SON 290 mm, which correspond to 24.2%, 30.1%, 22.8%, and 22.8% of the annual total. As a compact descriptor of intra-annual variability, we report the coefficient of variation of monthly totals (CV = 0.306, based on population standard deviation), and we note the number of months exceeding 100 mm (7 of 12 months). These statistics are carried forward as descriptive inputs for later comparisons. Meteonorm provides monthly mean daily sunshine duration and astronomical daylength for Aghdam as hours per day. We retained these daily means in their native units, then derived monthly totals by multiplying each monthly mean by the number of calendar days in that month, using a non-leap year for day counts. The sunshine fraction was computed as the ratio of monthly sunshine hours to monthly astronomical daylength, which is equivalent to the ratio of daily means because numerator and denominator scale by the same number of days. The monthly mean daily sunshine series, expressed in hours per day from January to December, is: 3.5, 3.5, 4.5, 6.0, 7.5, 9.0, 9.5, 8.5, 7.5, 5.0, 4.0, 3.5 h·day^{-1}. The corresponding astronomical daylength series in hours per day is: 9.0, 11.0, 12.0, 13.0, 14.0, 15.0, 15.5, 14.0, 12.0, 12.0, 10.0, 9.0 h·day^{-1}. After converting to monthly totals, sunshine duration equals 108, 98, 140, 180, 232, 270, 294, 264, 225, 155, 120, 108 h·month^{-1}, and astronomical daylength equals 279, 308, 372, 390, 434, 450, 480, 434, 360, 372, 300, 279 h·month^{-1}. The monthly sunshine fraction is therefore 38.9%, 31.8%, 37.5%, 46.2%, 53.6%, 60.0%, 61.3%, 60.7%, 62.5%, 41.7%, 40.0%, 38.9%. Annual aggregates were obtained by summation of monthly totals and yield 2195 h·year^{-1} of sunshine out of 4458.5 h·year^{-1} of astronomical daylength, which corresponds to an annual sunshine fraction of 0.492. Monthly extremes are identified based on monthly totals, with July providing the maximum sunshine (294.5 h) and February the minimum (98 h). Seasonal totals, computed using DJF, MAM, JJA, and SON groupings, are 315, 552, 828, and 500 h of sunshine against 866.0, 1196.0, 1364.5, and 1032.0 h of astronomical daylength, which correspond to seasonal sunshine fractions of 0.364, 0.462, 0.607, and 0.484. These quantities are used in subsequent analyses to relate available bright sunshine to potential photovoltaic energy yield on a monthly and seasonal basis. The intra-monthly variability of daily global horizontal irradiation was characterized for Aghdam using monthly values extracted from Meteonorm, reported as the minimum, maximum, and typical daily totals for each calendar month (all in kWh·m^2·day^{-1}). These three values represent, respectively, the lowest

and highest daily sums observed within the month as well as a central estimate that is representative of typical clear or average conditions. The range width, calculated as the difference between the maximum and minimum daily totals for each month, was used as a primary indicator of within-month variability. Across the annual cycle, the lowest daily irradiation values occur in December and January, while the highest are recorded in June and July. The month of May exhibits the greatest intra-monthly spread, with a minimum of 3.5, a maximum of 7.5, and a range width of 4.0 $kWh \cdot m^2 \cdot day^{-1}$. In contrast, December has the narrowest range, with daily totals spanning from 1.5 to 2.6 $kWh \cdot m^2 \cdot day^{-1}$. Typical daily values range from 2.1 $kWh \cdot m^2 \cdot day^{-1}$ in December to 7.8 $kWh \cdot m^2 \cdot day^{-1}$ in July. To quantify the general scale of variability, the average relative range width (defined as the ratio of range width to typical value) is 0.56, and the average ratio of maximum to minimum daily total is 1.94. These indicators provide a basis for assessing the expected daily spread in solar resource availability for each month, informing both photovoltaic system sizing and performance modeling. Monthly climatological means of daily maximum and minimum air temperatures for Aghdam were obtained from Meteonorm, with values representing typical conditions at 2 meters above ground level. For each month, the dataset provides the mean of all daily maxima and the mean of all daily minima, allowing calculation of the mean diurnal temperature range as the difference between these two values. The monthly mean maximum temperatures vary from 8.0 °C in January to 33.0 °C in July, while monthly mean minimum temperatures span from 0.0 °C in January to 22.5 °C in July and August. The annual average of the monthly mean maximum temperatures is 20.5 °C, and the annual average of the monthly mean minimum temperatures is 11.7 °C. The mean diurnal temperature range, averaged over all months, is 8.8 °C. The largest mean diurnal range is observed in July (10.5 °C), while the smallest occurs in December (6.5 °C). Seasonal aggregation was performed by averaging the corresponding months for each meteorological season. In winter (December to February), the mean daily maximum is 10.0 °C, the mean daily minimum is 2.5 °C, and the mean diurnal range is 7.5 °C. In spring, these values are 19.0 °C, 9.0 °C, and 10.0 °C, respectively. For summer, the averages are 31.3 °C for daily maxima, 21.5 °C for minima, and 9.8 °C for the diurnal range. In autumn, the values are 21.7 °C, 13.8 °C, and 7.8 °C, respectively. These temperature statistics provide the thermal context for evaluating temperature-dependent photovoltaic performance and are used directly in performance modeling and climate characterization for Aghdam.

3. Conclusion

Global and diffuse horizontal irradiation in Aghdam reveal a pronounced annual pattern, with the highest values recorded in June and July and the lowest in December and January. The annual sum of global horizontal irradiation exceeds 1500 $kWh \cdot m^{-2}$, while the diffuse component accounts for nearly half of this total. The diffuse fraction is most pronounced in spring months, peaking in April, and then gradually declines as the direct component becomes dominant during summer. Monthly air temperature values increase steadily from winter through summer, reaching a maximum in July and then declining towards the end of the year. The annual mean temperature remains moderate, but the amplitude between winter minimum and summer maximum exceeds 23 °C. Summer months consistently display average temperatures above 25 °C, while January records the lowest monthly mean, below 4 °C. Precipitation demonstrates significant variability throughout the year. The highest monthly totals are observed in December and May, while the driest month is January. Spring is the wettest season overall, followed by winter and the two drier seasons of summer and autumn. The annual precipitation sum exceeds 1200 mm, with more than half of the months recording totals greater than 100 mm. Sunshine duration also follows a clear seasonal rhythm. The maximum monthly sunshine is observed in July, with totals approaching 300 hours, while February has the lowest sunshine duration, under 100 hours. The annual sum of bright sunshine exceeds 2100 hours, and the fraction of actual sunshine to astronomical daylength is greatest in summer, reaching values above 60%. Intra-monthly ranges of daily global irradiation widen during the late spring and early summer, particularly in May and June, where daily totals can vary by up to 4 $kWh \cdot m^{-2} \cdot day^{-1}$ within the same month. Winter months such as December show both the lowest daily values and the smallest variability, with daily totals tightly grouped between 1.5 and 2.6 $kWh \cdot m^{-2} \cdot day^{-1}$. Analysis of monthly series of daily maximum and minimum air temperatures indicates that July records the highest mean daily maxima and minima, with values of 33.0 °C and 22.5 °C, respectively. In contrast, January minima approach 0.0 °C. The mean diurnal temperature range is widest in July, exceeding 10 °C, and narrowest in December. The combined seasonal cycles of irradiation, temperature, precipitation, and sunshine define a climate regime characterized by strong summer maxima, pronounced spring and late autumn transitions, and a relatively stable but subdued winter period.

References

[1] D. Palmer, E. Koubli, I. Cole, T. Betts, T., R. Gottschalg, Satellite or ground-based measurements for production of site specific hourly irradiance data: Which is most accurate and where? Solar Energy, 165, 240–255, 2018. https://doi.org/10.1016/j.solener.2018.03.029

[2] E. Abbasov, Sustainable solution for increasing the share of solar photovoltaic usages on residential houses in Azerbaijan. Environmental Research, Engineering and Management, 71(4), 11–18, 2015. https://doi.org/10.5755/j01.erem.71.4.12070

[3] J. Remund, S.C. Müller, M. Schmutz, P. Graf, Meteonorm Version 8. In Proceedings of EUPVSEC 2020.
[4] D. Yang, Solar radiation on inclined surfaces: Corrections and benchmarks. Solar Energy, 136, 288–302, 2016. https://doi.org/10.1016/j.solener.2016.06.062
[5] J.I. Wiltink, H. Deneke, Y-M. Saint-Drenan, C.C. Van Heerwaarden, J.F. Meirink, Validating global horizontal irradiance retrievals from Meteosat SEVIRI at increased spatial resolution against a dense network of ground-based observations. Atmospheric Measurement Techniques, 17, 6003–6024, 2024. https://doi.org/10.5194/amt-17-6003-2024
[6] S. Cros, J. Badosa, A. Szantaï, M. Haeffelin, Reliability predictors for solar irradiance satellite-based forecast. Energies, 13(21), 5566, 2020. https://doi.org/10.3390/en13215566

A.A. Guliyev, T.T. Asdanov, I.I. Hasanov, **Ecoenergetics, vol. 30, № 3, pp.15-19, (2025)**
https://doi.org/10.69624/Ecoenergetics.2025.3.15

Effects of Sliding Speed, Porosity, and Temperature on Copper-Alloyed Iron–Graphite Antifriction Materials

A.A. Guliyev, T.T. Asdanov, I.I. Hasanov

Azerbaijan State Oil and İndustry University, Baku, Azerbaijan,
aynur.sh84@mail.ru

Abstract. This article focuses on the investigation of the tribomechanical properties of iron-based antifriction materials alloyed with copper and reinforced with graphite additives, intended for use in friction joints operating under dry conditions. The study primarily examines how the coefficient of friction, wear rate, and surface temperature depend on different sliding speeds and porosity levels under oil-free loading. It was found that the reduction of porosity in the material after sintering leads to an increase in hardness. In other words, hardness after sintering is mainly determined by porosity and is not influenced by the initial particle size of the powder. It was also clarified that smaller particle sizes result in greater shrinkage during sintering. The research further revealed that increasing the pearlite content in the structure from 20% to 100% can enhance operational performance by approximately 1.5 times. One of the most noteworthy findings of the study is that the introduction of copper-alloyed graphite exhibits a complex effect compared to pure iron and iron–graphite systems. In this case, graphite acts simultaneously as a lubricating agent and copper serves as an alloying element, resulting in significantly improved overall material properties.

Keywords: sliding bearing, friction joint, iron-based material, graphite, copper-alloyed graphite, sliding speed, coefficient of friction, wear, temperature.

Corresponding author, email: *aynur.sh84@mail.ru*

1. Introduction

The regulation of the complex properties of all manufactured powder-based materials is one of the most important tasks in materials science. Depending on the operating conditions of household appliances and various industrial systems, the materials and components used in these applications are produced with different levels of porosity. During service, their tribotechnical properties must be thoroughly investigated. Numerous well-known research studies and the detailed analysis of the manufacturing technologies of the examined components significantly facilitate the development of new parts and expand their application fields. The availability of materials with diverse properties—most importantly, mechanical characteristics—allows them to be used in a wide range of engineering applications [1]. By controlling porosity, components operating in friction pairs acquire antifriction properties, since porosity plays a key role in the formation of stress concentrations. Particular attention is paid to the geometry of pores. For example, when 20–25% of the metallic cross-section of a material is replaced by pores—meaning that its effective load-bearing area decreases by the same proportion—the mechanical properties reduce approximately 2–5 times. Defects such as cracks, microcracks, and pore sphericity deviations formed during pressing are eliminated through repeated sintering. Many authors have attempted to establish mathematical relationships between porosity and mechanical properties in powder materials. The main goal of these studies is to ensure long-term serviceability of components made even from iron-based powders under real operating conditions. Within the allowable technological intervals of pressing, sintering, and other processing regimes, the properties of the materials can be regulated and optimized. Of course, these regimes may be adjusted to refine pore morphology and distribution [2]. In recent years, deformation strengthening characteristics of powder iron within certain porosity ranges have been studied, and porosity is additionally controlled through steam oxidation. The resulting strength, porosity, and density values are compared with their initial states. When powder materials are produced using powder metallurgy methods, dimensionless coordinates have increasingly been employed to describe the dependence of material properties on porosity. These coordinates allow researchers to generalize the relationship between porosity and changes in material characteristics. Using this method, both sintered and steam-oxidized powder materials can be monitored and directed toward suitable fields of application [3]. Today, reducing production costs of components used in any engineering field is achieved by optimizing the material properties. For example, in

household and industrial equipment—particularly in rotary compressors—the production of sliding bearing components such as cap–pad assemblies from powder materials and achieving high performance is an important technological challenge. The fabrication and operational justification of such components from powder-based materials has therefore become a highly relevant and contemporary research topic.

2. Experimental detail

For material selection, the powders obtained during experimental studies were analyzed, and new charge (charge-mix) materials to be compared with them were identified. The main objective in selecting suitable materials was to ensure the production of components with optimal physical-mechanical and tribomechanical properties while minimizing the use of expensive alloying elements. The previously known powder used for manufacturing the cap component was based on low-alloyed iron powder, which contained valuable metals such as Cu and Ni (grade ПРНD2). Producing components from such alloyed powders increases material cost significantly, making them impractical for large-scale industrial production. To overcome this limitation, the use of graphite alloyed with 6% copper was proposed. The introduction of copper-alloyed graphite allows the elimination of pure nickel and pure copper powders from the mixture, thereby reducing the overall cost of the powder blend while maintaining or improving the functional properties of the final component.

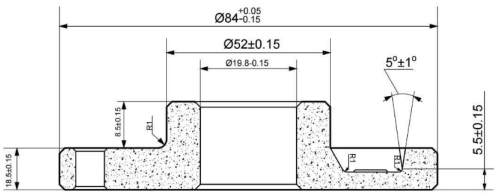

Figure 1. Working drawing of the powder-metallurgy cap–pad component

For the selection of material for the cap component (Figure 1), vacuum-processed iron powder was chosen as a more economical option. The composition of the charge mixture containing copper-alloyed graphite and its properties are presented in Table 1. The iron powder was produced by an atomization method and corresponded to grade ПЖРВ2, while the copper-alloyed graphite was manufactured using a specialized technology [4]. The morphology of the iron powder and the copper-alloyed graphite particles is shown in Figure 2. The chemical composition of the iron powder was as follows: Fe – base; C – 0.03%; Si – 0.10%; Mn – 0.3%; S – 0.2%; P – 0.02%. The powder particle size was selected as <0.20 mm. The apparent density of the iron powder was 2.6 g/cm³, and its true density was 6.9 g/cm³. The particle size of the copper-alloyed graphite powder was <200 μm [5]. The technological scheme for producing the powder-metallurgy cap–pad component is shown in Figure 3.

From the prepared powder mixture, samples were compacted using presses of models П-125 and HPM-100S at pressures of 400, 500, 600, and 700 MPa in a specially designed die. The dimensions of the test specimens were 10 × 10 × 55 mm. The sintering of both the specimens and the cap components was carried out not in the “Koyo Lindberg” furnace but in a CK3.4.40.0/11.5 furnace [6].

Table 1. Charge composition and physico-mechanical properties

Material grade	Chemical composition %			Density q/sm³	Porosity, %	Hardness HB, MPa	Coefficient of friction under lubricated conditions	Strength limit, MPa		
	Fe	C(Гр)	Cu (C)					Intension	Inbending	Incompression
Porous iron	100	-	-	6-6.5	15-25	400-550	0.07	160-120	180	300-400
ЖГр2	98	2	-	6.2-5.8	17-25	450-900	0.01-0.06	100	110	400
ЖГр2+6% МГ	92	2	6%	6.4-6.0	17-25	500-950	0.02-0.05	500-700	-	800-950

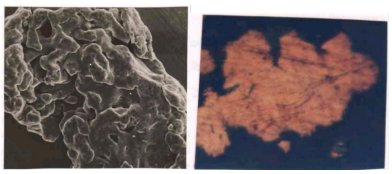

a b

Figure 2. Particle morphologies of iron and copper-alloyed graphite powders: a – iron powder, ×1000; b – copper-alloyed graphite powder, ×400

The relative sintered density is calculated using the following formula:

$$V=\rho_0/\rho_k \quad (1)$$

ρ_k - Density of the compact material of the base component, kq/m^3

Total porosity

$$П= (1 - \rho/\rho_k) \cdot 100\% \quad (2)$$

is calculated using the formula.

The additional porosity is determined in accordance with GOST 18898-73 by weighing the specimen in air and in water (hydrostatic method). Before weighing, the specimen is impregnated with oil under vacuum, after which the value is calculated using the specified formula.

$$П_a =(m_2 - m_1)100 \cdot \rho_s/(m_2 - m_3)\rho_y \quad (3)$$

m_1 - Weight of the specimen in air, in grams

m_2 ;m_3 - Weight of the oil-impregnated specimen in air and in water.

ρ_s density of water kq/m^3 ,1000 kq/m^3, ρ_y - density of oil -kq/m^3

In this study, U-20 oil was used for impregnation. Its ρ_y = 890kq/m^3, The closed porosity is calculated using Equation:

$$П_b =П_u - П_a \quad (4)$$

The drying of powders and specimens under vacuum conditions was carried out in a drying oven. The drying temperature was controlled using the oven's thermal regulator and was set within the range of 120–200°C. In addition to this method, the oil-impregnation process was performed using a laboratory-type apparatus. For metallographic investigations, the modern microscope model "Neophot-21" was employed. Hardness measurements were performed on a Rockwell hardness tester in accordance with GOST 9013. The tensile strength and yield strength of the specimens were determined using an IR-10 testing machine. The friction tests of the sintered specimens were conducted on the SMCh-2 machine following the standard methodology based on the "disk–pad" scheme. It was proposed to perform the friction tests under lubricated conditions (oil И-20) at sliding speeds of 4–12 m/s and pressures of 0.4–3 MPa [7, 8]. For specimens produced from pure iron powder, a friction path of 50 km within 6 hours of testing was adopted. The counter-specimen for the friction pair was manufactured from 45 steel, subsequently quenched and tempered to achieve a hardness of 38–42 HRC. The surface roughness was selected as Ra = 0.5 μm. In addition to prismatic specimens, the wear behavior of the finished sintered cap–pad component under operating conditions was examined using a specialized testing apparatus [9–10]. The results of the study showed that increasing porosity from 15% to 30% leads to a decrease in strength and impact toughness. Similarly, the influence of porosity on the physico-mechanical properties was demonstrated for the ЖГр2 + 6%МГ material (Figure 4). An increase in the pearlite content of the microstructure from 20% to 100% improves the operational performance of the material by nearly two times. This improvement is mainly attributed to the increase in strength and specific hardness. When the porosity reaches 30% and the microstructure consists of ferrite, ferrite–pearlite, or pearlite, the pressure limit at a sliding speed of 4 m/s is 7, 5, 9, and 12 MPa, respectively; however, at 10 m/s, the pressure limit decreases to 7.5 and 6 MPa. In softer (more ductile) ferritic and ferrite–pearlite structures, the increase in temperature leads to a reduction in both the allowable pressure and the structural factor. As the sliding speed increases, the load-bearing capacity during friction decreases, regardless of the material's microstructure. Under the given dry friction conditions, when the material porosity is 10%, the properties conform to those illustrated in the figure. When the ferrite content in the material reaches 20–30% (with hardness of 1300–1400 MPa), signs of seizure begin to appear, and both the wear intensity and the structural factor start to increase (Figure 6, curve 1).

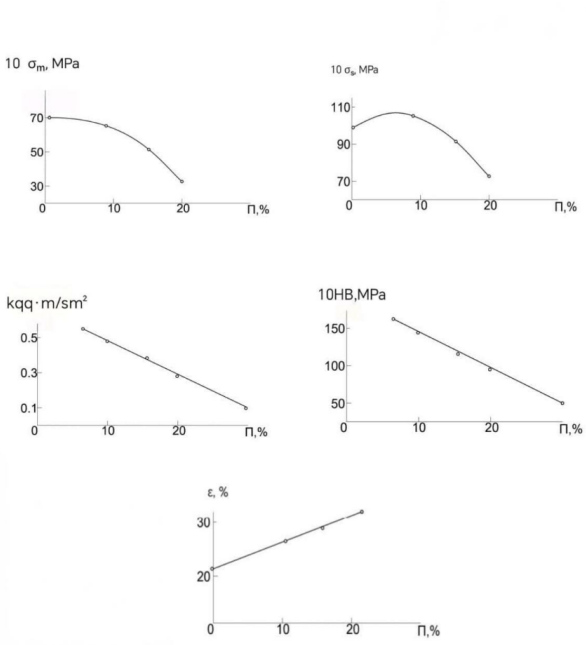

Figure 4. Effect of Porosity on the Mechanical Properties of ЖГр2 + 6%МГ Material

Description of the influence of porosity on the mechanical properties of the ЖГр2 + 6%МГ material (initial iron powder and copper-alloyed graphite particle sizes of 100 μm and <200 μm, respectively; microstructure: pearlite + cementite).

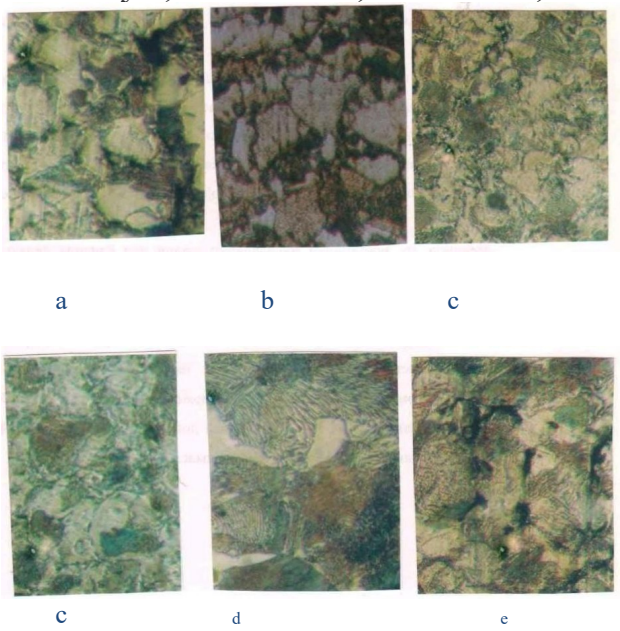

Figure 5. Microstructure of antifriction materials: a — alloyed ferrite; b — ferrite + pearlite; c — pearlite + dispersed cementite; d — pearlite + 3% cementite; e — pearlite.

In specimens with a pearlitic structure (hardness 1500–1600 MPa), high wear is observed, which increases with rising sliding speed (Figure 6, curve 2). In fine-grained pearlitic structures containing 12–15% cementite (Figure 5c), when the hardness reaches 2000–2200 MPa, the antifriction properties remain stable under the given sliding speed and loading conditions (Figure 6, curve 3).

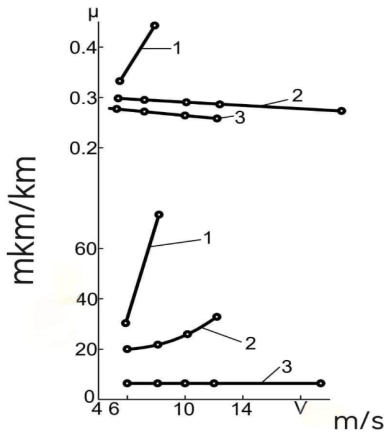

Figure 6. Dependence of the coefficient of friction and wear on sliding speed and microstructure for an iron-based material containing 3% graphite, 6% copper-alloyed graphite (MG), and 10% porosity at a load of 2 MPa: 1 — pearlite + 30% ferrite; 2 — pearlite; 3 — pearlite + 15% cementite.

The study revealed that, with increasing sliding speed, relatively lower friction coefficients, reduced wear, and lower surface temperatures are achieved when the material exhibits minimal porosity at the friction interface (Figure 7). Due to the presence of solid lubricants—graphite and copper-alloyed graphite—the material demonstrates long-term operational stability. The allowable load limits contribute to a reduction in frictional temperature (Tables 2 and 3). It was fully established that, for the antifriction cap–pad component operating under specific service conditions, there must be an optimal strength level and a minimum powder particle size. It was determined that the use of iron powder with particle sizes <100 μm and copper-alloyed graphite with particle sizes <200 μm plays a significant role in maintaining and regulating the antifriction properties of the material.

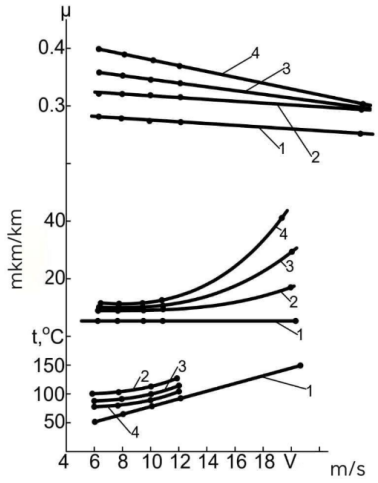

Figure 7. Dependence of the coefficient of friction, wear, and surface temperature on sliding speed and porosity (friction load: 2 MPa): 1 — 1% porosity; 2 — 10% porosity; 3 — 15% porosity; 4 — 20% porosity.

Table 2. Antifriction properties of ЖГр2 + 6%MQ iron–graphite material at different porosity levels (V = 4 m/s).

Actual porosity %	Density, q/sm^3	Average load limit, MPa	P=3 MPa, temperature °C	P=3 MPa Operating time, min
11.0	6.66	3.4	42.4	11;0
14.6	6.38	11.01	33.4	6;32
17.5	6.15	8.9	35.6	7;25
22.6	5.79	9.3	32.4	7;47
27.1	5.44	7.4	30.2	7;16
38.4	4.57	7.35	33.7	9;16

Table 3. Long-term self-lubricating performance of the cap–pad component produced from ЖГр3 + 6%МГ (P = 0.5 MPa, V = 4 m/s).

Porosity (%)	Oil absorption capacity (%)	Long-term operation (h)
19.4	1.42	5.0
21.2	2.07	15.0
24.0	3.13	17.5
27.5	4.10	17.0
30.8	5.08	10.0

The addition of copper-alloyed graphite to the iron–graphite material not only reduces porosity after sintering but also has a highly beneficial effect on mechanical properties—particularly hardness—and on other performance characteristics. This improvement plays a significant role in reducing the coefficient of friction. Therefore, the influence of the initial powder particle size is not as critical; rather, the reduction and proper regulation of porosity strongly affect both the mechanical and tribotechnical properties of the material.

3. Conclusion

The most significant improvement in the coefficient of friction and wear rate is achieved when the iron–graphite material contains surface-active solid lubricants as well as solid lubricants with metal deposited on their surface in the form of powder particles. This is confirmed by the high antifriction properties obtained in the present study when copper-alloyed graphite was introduced into the ЖГр2 iron–graphite powder material. Such additions promote the formation of a thin secondary tribolayer during friction, and the stability of this layer under dry sliding conditions enables the achievement of the lowest friction coefficients. The tribotechnical properties obtained in this work were established exclusively through experimental investigation. This represents one of the most accurate and realistic approaches within the scope of the study.

References

[1] A. T. Mamedov, Konstruktsionnogo i antifriktsionnogo poroshkovaya metallurgiya. Baku: Elm, 2005, 458 p.

[2] A. M. Dimitriev, “Issledovanie perspektivnykh tekhnologiy dlya krupnoseriynogo proizvodstva detalei iz poroshkovykh stalei,” Materialovedenie. Termicheskaya Obrabotka Metallov, no. 7, pp. 48–51, 2017.

[3] Poroshkovye iznosostoykie materialy na osnove zheleza: Materialy, poluchennye spekaniem i propitkoy poroshkovoy metallurgii, no. 1–2, pp. 44–53, 2001.

[4] A. V. SharifovaInfluence of electrochemical copper-coating regimes of graphite on the structure of the composite. In: Proceedings of the II International Scientific-Practical Conference on Modern Problems of Metal Physics, Baku, pp. 48–50, 2010.

[5] A. V. Sharifova and A. A. Quliyev, Comparative study of bearing materials for friction joints in household devices and the properties of friction pads. No. 1, 45–51, 2019.

[6] H. H. Eldarzade and A. A. Quliyev, “Ovuntu materiallarından hazırlanan hissələrin maşın ilə emalı,” Azerbaijan Higher Technical Schools Bulletin, no. 2, pp. 41–46, 2015.

[7] A. T. Mamedov, S. A. Jafarova, and A. A. Guliev, “Adaptation to the SMU-2 machine for determining tribotechnical characteristics of powder materials for construction purposes,” VII BOOK, no. 4, pp. 18–23, Baku.

[8] B. A. Abasov, B. B. Gafarov, and A. A. Guliyev, “Issledovanie pretekhnicheskikh svoystv metallicheskikh poroshkov, plankiovannykh razlichnymi sposobami,” in Proceedings of the International Conference on Science, Technologies and Small Business Development, Baku, 2000, pp. 163–165.

[9] S. M. Mustafaev, A. T. Mamedov, L. R. Salahova, and A. A. Guliyev, “Ustroystvo dlya tribotekhnicheskikh issledovaniy materialov i detalei v naturnom vide,” Trenie i Iznos, vol. 11, no. 1, pp. 742–745, 1990.

[10] A. T. Mamedov, A. A. Guliyev, V. V. Rumyantsev, and G. A. Gadzhiev, “Uzel k mashine modeli SMC-2 dlya ispytaniya detalei na iznos pri malykh nagruzkakh,” Trenie i Iznos, vol. 6, no. 3, pp. 554–559, 1985.

A. Ahmadov, **Ecoenergetics, vol. 30, № 3, pp.20-22, (2025)**
https://doi.org/10.69624/Ecoenergetics.2025.3.20

Analysis of the Causes of Drilling Pump Failures

A.Ahmadov

Azerbaijan State Oil and İndustry University, Baku, Azerbaijan,
alihikmat.ahmadov@asoiu.edu.az

Abstract. A drilling pump is a high-pressure, high-capacity reciprocating pump. High-pressure drilling pumps are the key components of the high-pressure drilling fluid delivery system. They function as the heart of the drilling fluid circulation system. The purpose of a drilling pump used on drilling rigs is to apply the required pressure to the drilling fluid during drilling operations. Various types of drilling pumps are used in drilling activities. The most used types in modern land-based operations are the duplex double-acting pump and the triplex single-acting pump. Over the past two decades, several new pump designs have been successfully implemented in drilling operations, particularly on offshore platforms. These newer pump designs include the quadruplex pump with four pistons (or plungers), the quintuplex pump with five pistons (or plungers), and the hexaplex pump with six pistons (or plungers).

Keywords: drilling pump; reciprocating pump; high-pressure pump; drilling fluid circulation; duplex pump; triplex pump; quadruplex pump.

Corresponding author, email: alihikmat.ahmadov@asoiu.edu.az

1. Introduction

The quadruplex and quintuplex pumps are structurally like triplex pumps in that they are single-row horizontal machines. The design of the hexaplex pump, however, is completely different. Its six single-acting pistons operate vertically and are arranged in a circular configuration; they are driven by a large cam rotated by a variable-frequency AC motor. The hexaplex pump has been developed primarily for offshore platforms, where the footprint of a single pump must be smaller than that of two triplex pumps. Smooth and uninterrupted operation of drilling pumps is critically important. Any shutdown caused by the failure of a key component results in the suspension of drilling operations. Failures of drilling pumps can be divided into problems related to the functioning of the mechanical section and the hydraulic section. The hydraulic section performs the pumping process and consists of several components, including valves, pistons, and liners (Fig. 1). These components are subjected to severe wear during operation, mainly due to cavitation effects. The drilling fluid used in drilling is a mixture of liquid substances and chemical additives. The fluid returning from the wellbore undergoes a complex cleaning process and is then pumped back into the bottomhole assembly. Pump components become damaged when the fluid is insufficiently cleaned [1]. The failure rate strongly depends on the chemical aggressiveness of the additives introduced into the drilling mud. These additives improve drilling fluid parameters (viscosity, density, ability to wash away contaminants, dissolution properties, etc.). Chemical additives are essential for maintaining standardized wellbore conditions and ensuring well quality; however, in most cases, they behave aggressively, particularly toward the elastomeric elements of pumps. Typical failures in mud pumps include wear that leads to an increased clearance between the cylinder and the piston, as well as damage to the suction and discharge valves. During intensive drilling, the discharge valve may fail every hour or so. Leakage resulting from worn piston–cylinder assemblies have consequences, such as contamination of the cylinder water-cooling system (which becomes noticeable even with minor damage), because the water circulating in a closed loop returns to the cooling tank. Suction and discharge valve failures are more difficult to identify, as leaks caused by washing are not visible externally. Such failures often become noticeable only at a later stage, when maintaining consistent discharge pressure becomes challenging. In these cases, the pump must be shut down immediately and the faulty valve replaced. The difficulty, however, lies in determining which valve has failed or is malfunctioning.

2. Experimental detail

One of the methods used to assess the condition of a valve is the “listening method.” Unfortunately, these methods are far from accurate, unreliable, and require comparing acoustic signals from different operating units approximately every fifteen minutes. A drilling

pump operates at pressures up to 52 MPa, which makes this diagnostic method hazardous and associated with a high risk of injury to the operator. A drilling pump failure caused by a leaking valve can result in a complete shutdown of drilling operations, which is particularly dangerous when drilling in so-called hard formations. For a drilling company, one hour of suspended operations can translate into substantial financial loss.

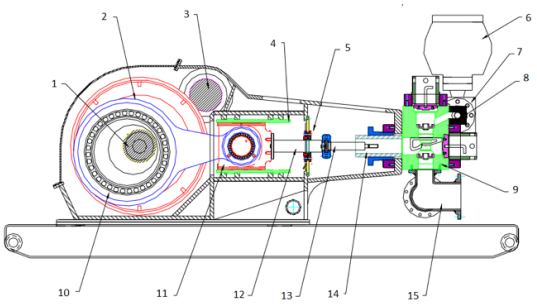

Figure 1. Schematic diagram of a drilling pump: 1 – crankshaft; 2 – main drive; 3 – gear; 4 – crosshead bushing; 5 – seal; 6 – compensator; 7 – filter; 8 – suction manifold; 9 – valve block; 10 – connecting rod; 11 – crosshead; 12 – extension rod; 13 – plunger; 14 – liner (cylinder); 15 – discharge manifold.

Modern researchers are conducting field studies on drilling pump valve failures aimed at developing and implementing a valve diagnostic system based on high-frequency elastic waves of acoustic emission. Preliminary results strongly indicate that such a system will be capable of detecting the early stages of valve damage, enabling personnel to plan timely repairs of the identified pump without shutting down the entire drilling operation. The hydraulic power generated by drilling pumps depends primarily on the geometric and mechanical configuration of the suction pipeline. Figure 2 illustrates an ideal layout with minimal friction and low inertia. A poorly designed pump suction line can result in increased hydraulic losses. Factors contributing to excessive friction in the suction line include sharp-edged inlet connections, filters installed directly at the pump entrance, suction pipes of small diameter, long sections of suction piping, and numerous fittings along the suction line. Minimizing inertial effects requires reducing the suction velocity and the weight of the drilling fluid. Usually, it is advisable to use a short suction pipe with a large diameter. When the desired suction conditions cannot be achieved, an auxiliary pump becomes necessary. This is a common solution used on many modern drilling rigs. The scientific work *"Assessment of the Negative Impact of High Bottomhole Temperatures on Wellbore Structural Elements and Drilling Equipment"* notes that problems may arise in drilling pumps due to overheating of the pumped fluid. A drilling fluid temperature of 150°C can create critical suction issues [2]. At low pressure or under vacuum inside the cylinder during the suction stroke, the fluid may begin to boil, which reduces suction efficiency. In addition, high-temperature drilling fluid accelerates the wear of rubber components, especially when oil is present. Large mud tanks with cooling surfaces typically solve this problem.

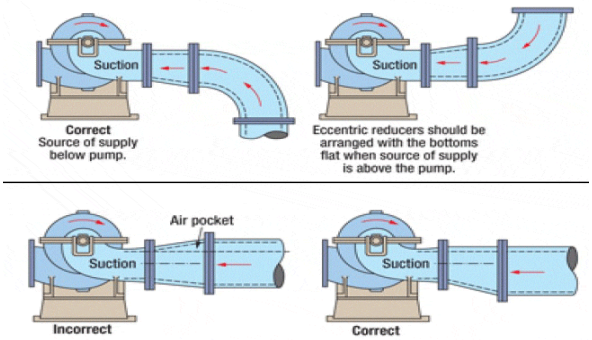

Figure 2. Design of hydraulic lines for a drilling pump.

The presence of gases in the drilling fluid also negatively affects the operation of the drilling pump. Dissolved gas and air expand under the reduced pressure during the suction stroke, thereby decreasing suction efficiency. Gas contained in water-based drilling fluids can also damage components made of natural rubber. Typically, the lubricating properties of the drilling fluid can be reduced when foreign solid particles are present—mainly sand and various types of hard minerals. To eliminate this issue, a shale shaker is used; through vibration, it removes abrasive particles from the fluid. According to studies described in *Underbalanced Drilling: Limits and Extremes (2012)*, a poorly designed discharge manifold can cause shock waves and excessive pressure fluctuations [3]. This manifold should be as short and straight as possible, avoiding sharp turns. A small atmospheric air chamber commonly equipped on pumps provides only moderate damping. For optimal performance, this air chamber should be supplemented with a larger air chamber or a pre-charged pulsation dampener.

3. Conclusion

Special solid materials such as limestone, expanded perlite, and others are commonly added to drilling fluids to fill or seal fractures within the wellbore. Most of these solid circulating materials can reduce the service life of pump components. They exert particularly strong effects on valves and seats when they accumulate on the valve seats or between the valve body and the valve disc. The elastomer seals on the piston are located inside ceramic or stainless-steel liners. The seals and liners are fast-wearing components, and most pumps are designed to provide easy access for maintenance and replacement of worn parts. Most pumps used in oilfield operations are triplex pumps. The reciprocating motion of the cylinders results in a non-uniform discharge flow,

which requires dampening to reduce vibration and component wear. In accordance with regulatory requirements, improvements in pump design and operational efficiency are primarily aimed at reducing mechanical and hydraulic losses. Therefore, further research aimed at developing a series of new structural and technological solutions to extend the service life of hydraulic components appears both promising and highly relevant. Such advancements would improve the manufacturing process from both economic and technical perspectives, and, consequently, would also have a direct positive impact on the drilling process.

References

[1] A. Bejger, Identification of structural defects of metal composite castings with the use of elastic waves, Archives of Metallurgy and Materials, 2011.

[2] V. V. Melnikov and A. V. Epikhin, Otsenka negativnogo vliyaniya vysokikh zaboynykh temperatur na elementy konstruktsii skvazhiny i burovoe oborudovanie, National Research Tomsk Polytechnic University, Tomsk, Russia, 2015.

[3] B. Rehm and A. Haghshenas, Underbalanced Drilling: Limits and Extremes. 2012.

V.H. Abdullayev, R.G. Abaszade, P.K. Dutta, et al., **Ecoenergetics, vol. 30, № 3, pp.23-26, (2025)**
https://doi.org/10.69624/Ecoenergetics.2025.3.23

Socio-Economic Transformation of Education in the Era of Industry 5.0

V.H. Abdullayev[1,2,3,4], R.G. Abaszade[1,2,3,4], P.K. Dutta[5], I.X. Normatov[3]

[1]Azerbaijan University of Architecture and Construction, Baku, Azerbaijan, abdulvugar@gmail.com
[2]Tashkent State Technical University named after Islam Karimov, Tashkent, Uzbekistan
[3]National University of Uzbekistan named after Mirza Ulugbek, Tashkent, Uzbekistan, ihnormatov@gmail.com
[4]Turan International Research Institute, Baku, Azerbaijan, abaszada@gmail.com
[5]Amity University, India

Abstract. The appearance of the industry 5.0 era is a paradigm shift of an innovative combination of technologies, sustainability and sustainability, and mankind. This paper discusses socio-economic change of education in this regard; mainly highlighting policy change, curriculum devolution as well as skill-building. It brings to the fore an interpenetration of green finance, technological innovation, and stakeholders' engagement with competence-based learning, STEAM education and SDGs alignment. The results highlight that flexibility, sustainability, and cross-sectoral collaboration is key to getting the most out of the benefits of Industry 5.0 in the socio-economic sense.

Keywords: Industry 5.0, Socio-economic transformation, Education reform, STEAM education, University–industry–government cooperation, Innovation ecosystem.

Corresponding author, email: abaszada@gmail.com

1. Introduction

Industry 5.0 represents the latest stage in the evolution of industries as it is characterized by the combination of high technologies and human-oriented and environmentally friendly technologies and processes. Industry 5.0 is a new stage in the development of the industrial environment and a combination of high-tech with human values and principles of sustainable development [1-4]. The change does not affect the manufacturing industry only, but it also has a significant impact on the education system to align with the developing socio-economic interests [5-7]. In this respect, companies have an obligation to focus on environmental sustainability as a central issue in all their strategies, especially those that are energy-intensive and tend to have heavy environmental loads [1,3]. Surplus capacities in production are an example of environmental waste, and its elimination can yield not only a positive impact but also a chance to enter the market competitors within the scope of differentiation and technological leadership [3]. The co-operation of the various stakeholders, i.e., governments, industry sectors, and institutes of higher learning and production is the common denominator of Industry 5.0 to build regional industrial brands and establish sustainable systems of innovation [4]. Financial openness also facilitates high-quality growth in manufacturing as it gives it increased access to capital markets, which subsequently drives technological advancement and eliminates funding issues [5]. In the education sector, to ready the workforce towards Industry 5.0, both technical and soft skills that include, programming, digital communication, problem, and creative, and adaptable skills would need to be incorporated into education curricula, based on cross-stakeholder training efforts [6,8]. Besides, the Triple Helix model of the integration of university, industry and government, becomes a critical model to enhance the efficiency of innovation, balancing between scientific, industrial and policy contributions to enhance regional competitiveness [14,15].

2. Experimental detail

The currents paradigm of Industry 5.0 lies between the advanced technology, the principles of sustainability, and human-center and approaches in the manufacturing industry, the focus of which is personalization, resilience, environmental accountability [3]. Among the characteristics of this industrial transition, there are environmental sustainability and green finance considerations, which guarantee the long-term healthy operation of companies as well as bring the production activities in

line with the Sustainable Development Goals [1,3]. The example of the application of Pichia kudriavzevii in the processing of waste-derived substances in bio-based manufacturing can also display the efficient ability of advanced biotechnology to decrease its environmental footprint and increase product sustainability throughout its lifecycle [2]. Artificial intelligence (AI) and machine learning allow highly specialized productions in terms of the production solution, enhance operating agility and responsiveness to changing consumer needs, and drive up the significance of highly skilled human labor. The regional competitiveness toward Industry 5.0 depends on green finance, innovation capacity and favorable institutional systems because they are vital in gauging changed advancement throughout industry worth chain [1]. Simultaneously, ethical factors like the balance between automation and human labor and the protection of the employees also mean that businesses are forced to invest in upskilling programs to equip the workforce with the task of this new industrial age [4]. To draw a conclusion, Industry 5.0 represents the synergy of the priorities of sustainability, technological innovation, and people-centric approaches being based on environmental responsibility and cooperative partnerships. Through such concepts, businesses have the potential to accelerate economic development at the same time stimulating societal and environmental resilience (Table 1).

Table 1. Key Components of Socio-Economic Transformation of Education in the Era of Industry 5.0

Section	Focus Area	Key Points	Expected Outcomes	Key References
Characteristics of Industry 5.0	Sustainability, human-centric innovation, and advanced manufacturing	Green finance integration, collaborative stakeholder networks, bio-based materials, AI-driven personalization	Environmentally sustainable industrial practices, innovation-driven economic growth	[1,2,5]
Directions of Socio-Economic Transformation in Education	Educational reform and modernization	Competency-based curricula, strengthening STEAM and digital literacy, SDG-aligned education	Skilled workforce with interdisciplinary and ethical competencies	[7,10]
New Skills Required	Workforce adaptability and technological proficiency	Technical skills (AI, robotics, low-carbon tech), soft skills (creativity, collaboration, adaptability)	Industry-ready professionals capable of human–machine collaboration	[6,8,9]
Social Impacts	Equality and opportunity expansion	Equal access to quality education, career diversification, regional knowledge exchange	Reduced socio-economic disparities, innovation diffusion	[6,7]
Integration Model	University–industry–government cooperation	Triple helix model, collaborative innovation policies, funding mechanisms	Strengthened innovation ecosystem and sustainable regional development	[11,13,14,15]

2.1 Directions of Socio-Economic Transformation in Education

2.1.1 Renewal of Educational Programs (Competency-Based Approach)

The increased emphasis on a competency-based approach values other thing more such as measurable skills and applied knowledge instead of rote learning. Curriculum is redesigned towards problem-solving, critical thinking, creativity, and adaptability to have graduates who can fulfil the versatile needs of the industry 5.0. This model focuses on outcomes of learning, more flexible forms of assessment, and incorporation of real-life case studies within curriculum.

2.1.2 Strengthening STEAM and Digital Literacy

Interdisciplinary thinking and innovation are also linked to the significance of an enlarged provision of Science, Technology, Engineering, Art, and Mathematics (STEAM) in learning. Besides the technical ability, digital literacy, which incorporates data analysis, cybersecurity knowledge, and AI tool application also enables the learners to become viable members of the digital economy. A program that teaches coding, robotics and design thinking in school and university prepares students to be ready to work alongside machines.

2.1.3 Education Aligned with Sustainable Development Goals (SDGs)

It would be very necessary to enshrine SDG principles to make socio-economic transformation more inclusive and sustainable through education. The curriculum is supposed to be revised with the view of emphasizing the environmental responsibility, social equity and global citizenship. The project learning of the renewable energy, circular economy, and ethical AI give students the knowledge and values they require to help solve the global problems and benefit the national developmental agenda.

2.2 New Skills Required for Industry 5.0

The development of Industry 5.0 has become another milestone in industrial trends, since it demands a

reassessment of workforce competencies to

be in unison with new technological and socio-economic requirements. With the industries that feel the force of high-tech technologies shifting toward the humanity-oriented approach, it is important to outline the skills that will be necessary to take an active part in the new environment. An increasingly large literature exists that can formulate a guide to comprehending the complex dexterities that will characterize the workforce in Industry 5.0. The medium and long-term focus on the achievement of carbon neutrality and sustainable production of energy sources imply the necessity of concentrating the skills in low-carbon technologies and their applicability in the market, which presupposes changes in the curriculum of educational institutions [10]. The training builds technical skills as well as employability since the competencies of the graduates are aligned to the needs of the industry. Relating the concept to the technical and vocational education field, there is more and more emphasis by the employers on the balance between hard skills, including the advanced ability to work with the technical equipment, and soft skills, consisting of the ability to communicate and work in the team [10]. Both sets of skills make the workforce capable of functioning within the interdisciplinary environment of Industry 5.0. In the end, creating flexibility and technology and interpersonal skills will require academic, industry and policy maker collaborations that will be necessary to succeed in a sustainable, digital connected industry world.

2.3 Social Impacts

2.3.1 Strengthening Educational Equality

The issue of distribution of quality learning resources becomes less discriminative as Industry 5.0 technologies are added to education. Digital platforms, adaptive learning systems, and distant instructional models make sure that rural and urban students obtain equal amounts of teaching quality. This creates an atmosphere of inclusivity and stays in line with the notion of people of all social groups undergo lifelong learning.

2.3.2 Expansion of Career Opportunities

The changeover to technology-driven economy where people are put at the center brings about novel job types as well as enhancing inter sectoral mobility. In Industry 5.0 aligned education, the learner is provided with a multidisciplinary skills base, thus forming access to advanced manufacturing, sustainable energy, artificial intelligence powered services, and creative industry roles. Such cross-training of career paths enhances the employment flexibility of the workforce in uncertain markets.

2.3.3 Knowledge Exchange Between Regions

Real-time transmission of knowledge, research results and education materials can be shared and exchange across geographies using digital connectivity and collaborative platforms. This helps share best practices, facilitates collaborative academic

projects and serves to share and exchange cultures as well as professions. Subsequently, regional disparities in knowledge capital become minimized, and national innovation capacity are enhanced.

2.4 Integration Model

2.4.1University–industry–government cooperation.

The complex interaction between universities, industry and governments is critical in the context of driving innovation, improved economic progress and the creation of a knowledge-based economy. The triple helix one could call it has become prominent in the recent past years, a way to look at how a synergy between these three sectors can produce significant technological and innovative transformation. In this synthesis, I will take an in-depth front at the mechanisms, challenges, and implications of the collaboration of the university, industry, and the government as elucidated by different research (Figure 1).

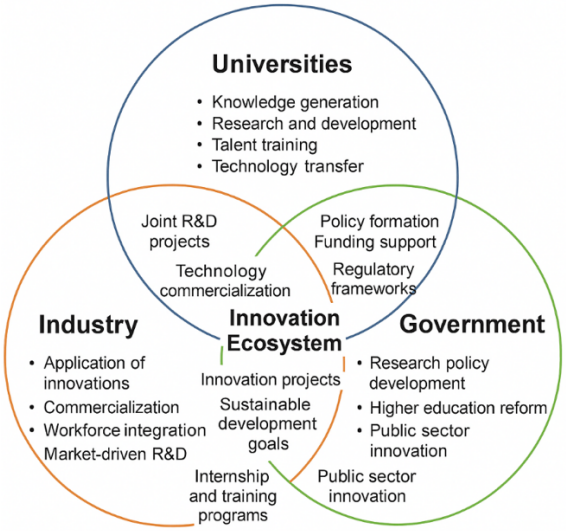

Figure 1. Triple Helix Model for University–Industry–Government Cooperation in the Era of Industry 5.0

Due to the implementation of the Triple Helix model in Industry 5.0, co-creation among the university, industry, and government occurs strategically, providing an opportunity to use scientific knowledge, commercialize technologies, and develop a sphere of innovations. There is a mutually reinforcing system in that universities are domains of knowledge, industry is solution-oriented to the market, and the government supports it by regulation and financing (Sun, 2007; Nam et al., 2019). A base of policies, clear funding methods, and equal access to digital environments are key to successful collaboration, whereas cross-functional ties bring much more excellent results in innovation (Hossain et al., 2011; Zhuang et al., 2021).

The maintenance of such advantages needs life-long learning, flexibility, and holistic stakeholder collaboration to enhance the country social-economic resilience, and competitiveness.

3. Conclusion

Industry 5.0 is a new stage of industrial development and a shift in the socio-economic performance of education, which implies not only the integration of the most innovative technologies but also humanistic values, sustainability, and collaborative innovation. The prescription of adaptation to the curriculum, teaching, and institutional collaboration patterns should be elaborate with an emphasis on competency-based learning, STEAM education, digital literacy, and addressing the Sustainable Development Goals (SDGs). Industry 5.0 workers do not only need technical knowledge but also creativity, adaptability, critical thinking and ethical responsibility to be able to work in the era marked by human-machine cooperation and sustainable technologies. These changes in education can help decrease inequality, increase opportunities in careers and enhance knowledge exchange with the help of the Triple Helix model in which universities, industry and government come together. Inclusive attitudes, resilient policies and positive theories of sustainability and demand will make education a driver of resilience, equity and long-term economic prosperity.

References

[1] C. Lin, X. Zhang, Z. Gao, and Y. Sun, "The development of green finance and the rising status of China's manufacturing value chain," *Sustainability*, vol. 15, no. 8, p. 6395, 2023, doi: 10.3390/su15086395.

[2] P. Pongcharoen, "The ability of *Pichia kudriavzevii* to tolerate multiple stresses makes it promising for developing improved bioethanol production processes," *Lett. Appl. Microbiol.*, vol. 75, no. 1, pp. 36–44, 2022, doi: 10.1111/lam.13703.

[3] H. Wang and B. Li, "Environmental regulations, capacity utilization, and high-quality development of manufacturing: An analysis based on Chinese provincial panel data," *Sci. Rep.*, vol. 11, 2021, doi: 10.1038/s41598-021-98787-y.

[4] X. Wang and L. Gao, "Research on the characteristics of multi-subject collaborative relationship based on the background of computer algorithm," 2023, doi: 10.4108/eai.19-5-2023.2334256.

[5] J. Wu and M. Zhang, "A systematic literature review of the empirical research on the promoting mechanism of high-level financial opening to innovative development of manufacturing industry," *J. Risk Anal. Crisis Response*, vol. 13, no. 1, 2023, doi: 10.54560/jracr.v13i1.357.

[6] K. Bremer and S. Maertens, "Future skills of flight attendants in times of COVID-19-related job uncertainty—The case of Germany," *Administrative Sciences*, vol. 11, no. 4, p. 154, 2021, doi: 10.3390/admsci11040154.

[7] A. Grenčíková, M. Kordoš, and V. Navickas, "The impact of Industry 4.0 on education contents," *Verslas Teorija ir Praktika*, vol. 22, no. 1, pp. 29–38, 2021, doi: 10.3846/btp.2021.13166.

[8] P. Oeij *et al.*, "A conceptual framework for workforce skills for Industry 5.0: Implications for research, policy and practice," *J. Innov. Manage.*, vol. 12, no. 1, pp. 205–233, 2024, doi: 10.24840/2183-0606_012.001_0010.

[9] K. Okoye and S. Nkanu, "Employers' identification of skills needed by technical and vocational education graduates for industrial work effectiveness," *J. Educ. Society Behav. Sci.*, pp. 32–41, 2020, doi: 10.9734/jesbs/2020/v33i230200.

[10] P. Rowley and C. Walker, "Adapt or perish: A new approach for industry needs-driven master's level low-carbon energy engineering education in the UK," *Energies*, vol. 13, no. 9, p. 2246, 2020, doi: 10.3390/en13092246.

[11] M. Hossain, J. Moon, H. Kang, S. Lee, and Y. Choe, "Mapping the dynamics of knowledge base of innovations of R&D in Bangladesh: Triple Helix perspective," *Scientometrics*, vol. 90, no. 1, pp. 57–83, 2011, doi: 10.1007/s11192-011-0507-6.

[12] G. Nam, D. Kim, and S. Choi, "How resources of universities influence industry cooperation," *J. Open Innov. Technol. Mark. Complex.*, vol. 5, no. 1, p. 9, 2019, doi: 10.3390/joitmc5010009.

[13] Y. Sun, "Collaborative research networks of Japanese universities: Bibliometric trends," *Collnet J. Scientometrics Inf. Manage.*, vol. 1, no. 2, pp. 7–13, 2007, doi: 10.1080/09737766.2007.10700825.

[14] T. Zhuang, S. Zhao, M. Zheng, and J. Chu, "Triple helix relationship research on China's regional university–industry–government collaborative innovation: Based on provincial patent data," *Growth Change*, vol. 52, no. 3, pp. 1361–1386, 2021, doi: 10.1111/grow.12490.

[15] T. Zhuang, Z. Zhou, and Q. Li, "University–industry–government triple helix relationship and regional innovation efficiency in China," *Growth Change*, vol. 52, no. 1, pp. 349–370, 2020, doi: 10.1111/grow.12461.

.

ECO

ENERGETIKA
ENERGETICS